U.S.N.A. --- Trident Scholar project report; no. 304 (2003).

ENVIRONMENTALLY ASSISTED CRACKING PROPERTIES OF AA7249 EXTRUSIONS FOR AEROSPACE APPLICATIONS

by

Midshipman Kristen L. Deffenbaugh, Class of 2003
United States Naval Academy
Annapolis, Maryland

_____
(signature)

Certification of Advisers Approval

Assistant Professor Michelle G. Koul
Mechanical Engineering Department

_____
(signature)

_____
(date)

Associate Professor Angela L. Moran
Mechanical Engineering Department

_____
(signature)

_____
(date)

Acceptance for the Trident Scholar Committee

Professor Joyce E. Shade
Deputy Director of Research & Scholarship

_____
(signature)

_____
(date)

REPORT DOCUMENTATION PAGE

Form Approved
OMB No. 074-0188

1. AGENCY USE ONLY (Leave blank)	2. REPORT DATE	3. REPORT TYPE AND DATE COVERED
	2 May 2003	

4. TITLE AND SUBTITLE
Environmentally assisted cracking properties of AA7249 extrusions for aerospace applications

5. FUNDING NUMBERS

6. AUTHOR(S)
Deffenbaugh, Kristen L.(Kristen Lynn), 1981-

7. PERFORMING ORGANIZATION NAME(S) AND ADDRESS(ES)		8. PERFORMING ORGANIZATION REPORT NUMBER

9. SPONSORING/MONITORING AGENCY NAME(S) AND ADDRESS(ES)		10. SPONSORING/MONITORING AGENCY REPORT NUMBER
US Naval Academy Annapolis, MD 21402		**Trident Scholar project report no. 304 (2003)**

11. SUPPLEMENTARY NOTES

12a. DISTRIBUTION/AVAILABILITY STATEMENT	12b. DISTRIBUTION CODE
This document has been approved for public release; its distribution is UNLIMITED.	

13. ABSTRACT: The Development of new military aerospace platforms is costly and time-consuming. Therefore, it is important that current platforms maximize their service lifetime. Exposure to environmental elements, particularly seawater, is especially troublesome to the Navy because it shortens required aircraft lifetime. The P-3C is an example of a versatile aircraft whose lifetime has been extended to the point that environmental attacks is now becoming a significant concern. Structural components in the P-3C are currently composed of aluminum alloy AA7075-T6, which has high strength but limited corrosion resistance. In particular, AA7075-T6 is susceptible to environmentally assisted cracking (EAC), which can cause catastrophic fracture of a stressed part. In 1999, Lockheed Martin Aeronautical Systems was granted funding to complete the Service Life Assessment Program (SLAP) for the P-3. One objective of this program was to identify a possible replacement for corrosion-prone AA7075-T6 extruded components that would help reach the goal service life of 2015. AA7249 is currently under development as a possible replacement material. The objective of this Trident project is to extend the ongoing evaluation of AA7249 extrusions to include corrosion testing, mechanical testing, and evaluations of the effects of processing on wide panel extrusions. The results of this study will contribute to the ongoing evaluation of these alloys for replacement of AA7075-T6 in aerospace structures and contribute to a better basic understanding of the structure/property relationship obtained for these component parts as well as the effect of processing on EAC behavior and material performance.

s

14. SUBJECT TERMS:	15. NUMBER OF PAGES
aging aircraft, AA7249, aluminum extrusions, environmentally assisted cracking, grain orientation, processing	**62**
	16. PRICE CODE

17. SECURITY CLASSIFICATION OF REPORT	18. SECURITY CLASSIFICATION OF THIS PAGE	19. SECURITY CLASSIFICATION OF ABSTRACT	20. LIMITATION OF ABSTRACT

Abstract

Development of new military aerospace platforms is costly and time-consuming. Therefore, it is important that current platforms maximize their service lifetime. Exposure to environmental elements, particularly seawater, is especially troublesome to the Navy because it shortens required aircraft lifetime. The P-3C is an example of a versatile aircraft whose lifetime has been extended to the point that environmental attack is now becoming a significant concern. Structural components in the P-3C are currently composed of aluminum alloy AA7075-T6, which has high strength but limited corrosion resistance. In particular, AA7075-T6 is susceptible to environmentally assisted cracking (EAC), which can cause catastrophic fracture of a stressed part. In 1999, Lockheed Martin Aeronautical Systems was granted funding to complete the Service Life Assessment Program (SLAP) for the P-3. One objective of this program was to identify a possible replacement for corrosion-prone AA7075-T6 extruded components that would help reach the goal service life of 2015. AA7249 is currently under development as a possible replacement material. The objective of this Trident project is to extend the ongoing evaluation of AA7249 extrusions to include corrosion testing, mechanical testing, and evaluations of the effects of processing on wide panel extrusions. The complete study is executed in three phases: (1) evaluation of local properties such as hardness, strength, and electrical conductivity as a function of position within the extrusions, (2) characterization and quantification of the EAC resistance as a function of the grain structure via slow strain rate technique, and (3) evaluation of the microstructure (i.e. grain shape and orientation) as a function of position within the extrusions. The results of this study will contribute to the ongoing evaluation of these alloys for replacement of AA7075-T6 in aerospace structures and contribute to a better basic understanding of the structure/property relationship obtained for these component parts as well as the effect of processing on EAC behavior and material performance.

Keywords: aging aircraft, AA7249, aluminum extrusions, environmentally assisted cracking, grain orientation, processing

Acknowledgements

Over the past year, many people have assisted me and without their help, I would not have had much success. I would like to thank those people who have shared with me both their expertise and time.

I would like to thank Dr. William Frazier (Naval Air Warfare Center - Aircraft Division), Dr. Eui Lee (Naval Air Warfare Center - Aircraft Division), and Dr. Omar Es-Said (Loyola Marymount University) for their support over the summer while I was at Patuxent River Naval Air Station for an internship. Their expertise in aluminum alloys provided an excellent starting ground. They also were able to show me the vital connection between how research becomes military application.

While down at Patuxent River, I was also able to spend an entire week in the Thermal Lab with Mr. Robert Boswell. I would like to thank Mr. Boswell for not only providing the space and time to conduct my tests, but also for teaching me about the theory and procedures involving differential scanning calorimetry. In addition, thanks go to the USNA Chemistry Department for allowing me access to their DSC unit.

Dr. Iulian Gheorghe (ALU Menziken Aerospace / Universal Alloy Corporation) not only provided us with the 2-inch extruded bar, but a thorough tour of the facilities during which he taught me about the extrusion process. In addition, he was always helpful with any questions I had. Spectrulite Corporation, despite labor and financial difficulties, graciously provided the wide panel extrusion.

I would also like to express my appreciation for the support I found around the Naval Academy in completing my project. Mr. Tom Price and the machine shop technicians were always very willing to work with me in preparing my samples for testing. I would also like to thank Professor Jim Joyce for teaching me how to run fatigue tests to precrack specimen.

Assistant Research Professor Brian Connolly provided a great amount of assistance in running the double cantilever beam tests. I would like to thank him for helping me to understand the theory, setup, and procedures in addition to the many hours he dedicated.

My family has also been there for me throughout the course of the year. They were very understanding and always willing to encourage me when I needed it.

I would especially like to thank Mr. Butch Antenucci and Mr. Steve Crutchley for their help in the Materials Lab. Not only would they teach me whatever I asked about, they were more than willing to drop whatever they were working on and lend a hand at any time. In addition, I would like to thank Miss Rachel Carr for her assistance in the lab throughout the year.

Finally, my advisors throughout the year have been Assistant Professor Michelle Koul and Associate Professor Angela Moran. I would like to express my most sincere appreciation for all the assistance they gave me throughout the year. Their constant and never ending support truly made this experience incredible. Professor Koul's sincere interest and passion for her work kept me motivated and always moving. Professor Moran always kept me on track and focused. I greatly appreciate both of their never-ending patience and willingness to always be there. Not only did they make this huge learning experience very enjoyable, but they inspired me with their dedication and passion for their work.

Table of Contents

List of Figures and Tables

Background

The Problem of Corrosion

The Cost of Corrosion

Corrosion is a natural process that occurs when a material is exposed to an environment in which oxidation of the material is thermodynamically favorable. Despite different control methods such as coatings and inhibitors, corrosion still has a considerable economic impact. A two-year study was recently completed by the U.S. Federal Highway Administration to provide a cost estimate of the impact of corrosion. This study, initiated by the National Association of Corrosion Engineers (NACE) International, was not only to determine an estimate of the cost, but also to identify methods to minimize the impact of corrosion in industry. This study revealed that approximately 3.1% of the Gross Domestic Product (GDP), or $276 billion dollars is spent directly on corrosion.[1] Of the approximately $137.9 billion spent per year on corrosion in industry, $29.7 billion is spent on transportation. Aircraft alone accounts for 7% (in excess of $2 billion per annum) of the total cost of corrosion in transportation. This estimate accounts for design, maintenance, and downtime of the aircraft.

As procurement of both military and commercial aircraft slows and many of these aircraft approach or surpass 20 years in service, inspections become more frequent and maintenance is performed more often to maintain service. Although corrosion cannot be eliminated, it is estimated that 25-30% of the money spent on corrosion could be saved with improved management techniques.[2]

Aging Aircraft and Its Effect on the Navy

By the year 2003, the projected average age for U.S. Naval aircraft will be 20 years.[3] Research and development of new platforms occur on a regular basis. However, this is very costly and time consuming; thus, until these replacements are available, the current platforms are required to remain in service. The majority of these aircraft in service for both the U.S. and NATO forces are older aircraft.[4] As many of these aging aircraft begin to approach their service lifetimes and as these lifetimes are extended, the issue of maintaining the aircraft becomes increasingly important.

Two major factors contribute to the "aging" of aircraft: fatigue and corrosion degradation. Fatigue degradation, a direct result of aircraft use for specific loads and conditions, can be accounted for in the original design. Corrosion degradation is less predictable due to a wide variety of controlling factors. The Navy, in particular, operates in extreme environments in which aircraft are consistently exposed to corrosives such as seawater, exhaust fumes, and humid environments. These conditions, combined with limited space and resources aboard ship, press the Navy to find ways to control the influence of corrosion through materials selection, processing, or heat treatment.

The P-3C Orion

Figure 1: The P-3C Orion is the Navy's primary anti-submarine aircraft.

The P-3 is the Navy's extended range, land-based platform used primarily for anti-submarine warfare. The most recent version of the P-3, as seen in Figure 1, is the P-3C Orion. The Orion serves in many roles including support of a carrier battle group, support of an amphibious readiness group, or solo missions.

The Orion was originally introduced into the fleet in 1969 with a service life goal of 7,500 hours. Although production ceased in 1990, the service life of the P-3C continues to increase.[5] The most recent service life assessment in 1998 increased the flight hours to 30,000 hours by the year 2015.[6]

In March of 1999, Lockheed Martin Aeronautical Systems was granted funds to conduct Phase II and III of the Service Life Assessment Program (SLAP). The goal of this program was to assess the characteristics of the airframe and to determine the modifications that could be made in order to reach the service goal life of 2015.[7] One of the deliverables requested by the Navy was a list of possible material replacements for the current high strength aluminum alloy on the P-3C Orion.

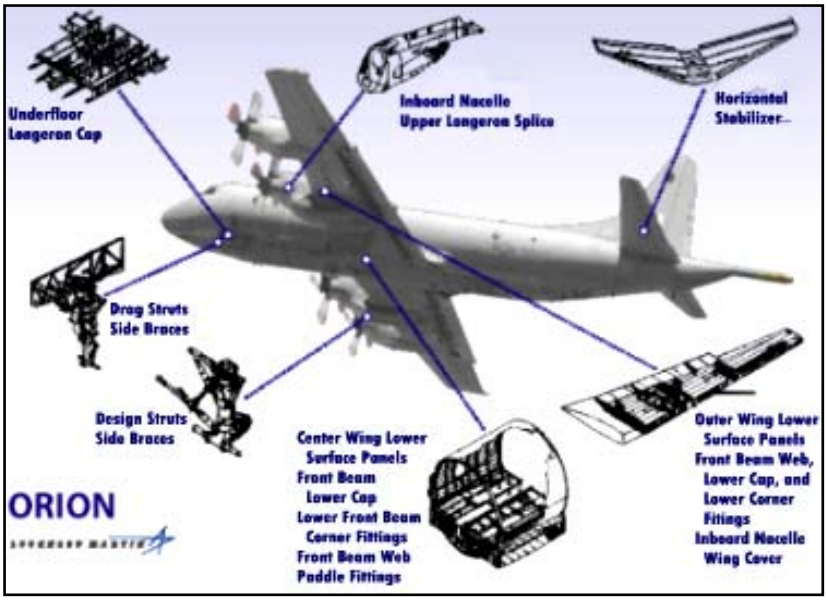

Figure 2: Several parts are being considered for drop-in replacement on the P-3C Orion.

High strength structural components on the Orion are composed of AA7075-T6. Although AA7075-T6 is a high strength alloy, its poor resistance to corrosion requires a large investment of both time and resources in prevention and maintenance in order to keep the P-3Cs flying. Figure 2 shows the locations of parts on the Orion composed of AA7075-T6.[8]

There are several proposed solutions to the problems involving AA7075-T6. Although some solutions involve improved heat treatments for AA7075[9], there are parallel efforts now aimed at finding a suitable replacement material for the problem parts. In order to gain an understanding of the depth of the problem, it is first necessary to understand the history of the development of modern aluminum alloys.

Development of High Strength Aluminum Alloys

Introduction to Aluminum

Aluminum has been employed in engineering applications since the end of the 19th century. The introduction of aluminum into engineering applications was in 1886, when Charles Hall and Paul Héroult developed an electrolytic method to reduce alumina (Al_2O_3) once it had been dissolved in molten cryolite.[10] This method, the Hall-Héroult process, had an incredible impact on a world where light-weight materials were needed for new engineering applications such as internal-combustion engines in vehicles and long-distance power transmission towers. In a few decades with the first flight of the Wright bothers, aluminum was introduced into the aerospace industry, where it has been employed ever since.[11]

Table 1: Designations for wrought aluminum alloys

Series	Alloying Element	Primary Uses
1XXX	Unalloyed	Electrical/Chemical Industries
2XXX	Cu	Aircraft
3XXX	Mn	Architectural applications
4XXX	Si	Welding rods; brazing sheet
5XXX	Mg	Boat hulls; gang planks
6XXX	Mg and Si	Architectural extrusions
7XXX	Zn	Aircraft; high-strength applications
8XXX	Sn or Li	Miscellaneous
9XXX	---	Reserved for future use

Aluminum alloys can be divided into two major categories: casting compositions and wrought compositions. In the United States, the Aluminum Association has further subdivided both casting and wrought compositions into families. Each of these families, also known as series, is labeled with a four-digit designation and describes the composition of the alloy. As seen in Table 1, wrought compositions are broken into nine major series distinguished principally by the primary alloying element.

A suffix is added onto the end of the alloy designation signifying the temper of the alloy. A temper designation of "T" indicates that the alloy is strengthened by heat treatment. The additional numbers following the "T" describe the type of heat treatment applied to the alloy. A few of these designations are of particular interest concerning high strength aluminum alloys. Two specific tempers in discussing high strength aluminum alloys are T6 and T7. T6 describes an alloy that has been solution heat treated and subsequently artificially aged. T7 also involves solution heat treatment, but materials subjected to this temper are then overaged. The tempers create very different material properties especially in terms of strength and corrosion resistance.

History of High Strength Aluminum Alloys

During the 1940's, the discovery that the addition of zinc and magnesium to aluminum alloys led to higher strength as compared to the existing 2XXX series began the development of 7XXX series aluminum alloys. AA7075-T6 was first employed on the B-29 bomber during WWII and soon became the primary structural aluminum alloy due to its high strength.[12] As commercial airplanes were developed, the need for an alloy that had better corrosion resistance

led to the development of the T7X tempers.[13] These tempers improved the corrosion resistance of the T6, but did so at the expense of a 10% to 15% reduction in strength.

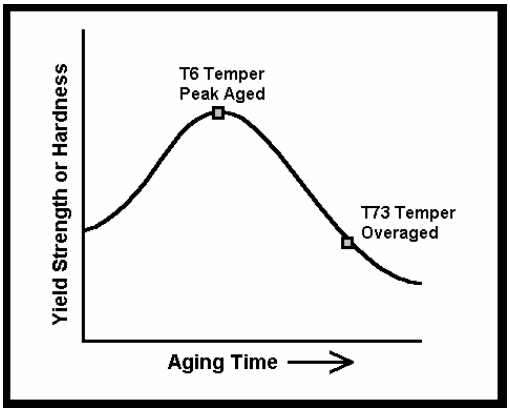

Figure 3: Schematic of the aging curve of the 7XXX series alloys

AA7075 is a heat-treatable aluminum alloy that is strengthened by precipitation hardening. Figure 3 shows the relationship between aging time and strength for 7XXX series alloys. 7XXX series aluminum alloys are strengthened by the precipitation of different precipitate phases, which, depending on their form, affect the strength and corrosion characteristics of the alloy. The primary precipitate of the 7XXX series alloys is $MgZn_2$ which can be found in two different crystalline structures, η'or η. The strength of the peak aged condition (T6 temper) is due to the formation of a combination of small, spherical Guinier-Preston (GP) zones (separate from the η'- and η– phases), the transition η'-phase, and the equilibrium η–phase. The coherent GP zones and coherent to semi-coherent η' are finely dispersed within the grains. The incoherent η are closely spaced along the grain boundaries. The microstructure of the T6 temper is dominated by finely dispersed η' precipitates. The large amount of these fine precipitates is responsible for the strength of the T6 condition.

As the alloy is further aged, it reaches the overaged (T7X) condition. In this condition, the $MgZn_2$ exists primarily as η, with some η' and coarsely distributed GP zones remaining. The remaining η precipitates, larger than those in the T6 temper, are located along the grain boundaries and are incoherent with the matrix. These η are thought to be responsible for the corrosion resistance of the T7X tempers.[14] Although the T7X temper has superior resistance to corrosion, it sacrifices approximately 15% of the peak age strength.[15]

Development of 7XXX Series Aluminum Alloys

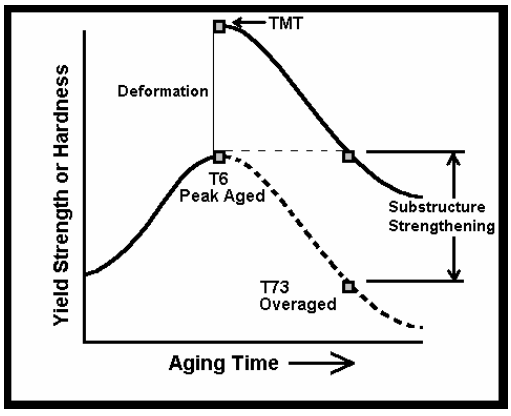

Figure 4: Schematic of the effect of FTMT on 7XXX Series Alloys

One possible solution in terms of improving the properties of AA7075-T6 is to apply processing techniques called final thermal mechanical treatments (FTMT). FTMT requires a combination of deformation with overaging to obtain an increase in strength and corrosion resistance. Figure 4 shows the relationship between the FTMT process and the aging process. The increase in strength is attributed to the superposition of strengthening effects due to mechanically induced structural defects (dislocations) and the introduction of precipitate phases; the increase in corrosion resistance is gained by obtaining favorable precipitate microstructure due to overaging.[16] Although this method showed promising results in the lab, it was never applied in the industry because of difficulties in controlling the production environment.[17]

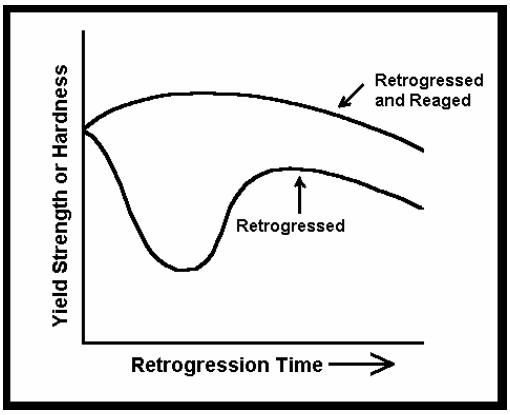

Figure 5: Schematic of the effect of RRA on 7XXX series alloys

In 1974, a new heat treatment was patented by Cina[18] referred to as retrogression and reaging (RRA). RRA involves three different steps: (1) a solution heat treatment above the solubility limit followed by a quench and artificial aging to produce the T6 temper, (2) a short heat treatment below the solubility limit followed by a quench, and (3) reaging similar to the aging of the T6 temper. Figure 5 shows the RRA process with respect to time. Initial retrogression causes a decrease in strength; the reaging recovers the strength of the T6 condition, and in some cases increases it to above the T6 condition. RRA results in a microstructure that has both the coarse η precipitates along the grain boundaries favoring high resistance to EAC and η' precipitates finely dispersed inside the grains favoring strength. The combination of both produces the favorable strength and corrosion resistance qualities of RRA treated material.[19,20]

The New Generation of 7XXX Series Aluminum Alloys

Table 2: Composition of selected 7XXX series alloys (given in % mass)

	7075	7150	7249
Zinc	5.1 - 6.1	5.9 - 6.9	7.5 - 8.2
Copper	1.2 - 2.0	1.9 - 2.5	1.3 - 1.9
Magnesium	2.1 - 2.9	2.0 - 2.7	2.0 - 2.4
Zirconium	---	0.08-0.15	---
Silicon	0.4	0.12	0.1
Iron	0.5	0.15	0.12
Manganese	0.3	0.1	0.1
Chromium	0.18-0.28	0.04	0.12-0.18
Titanium	0.2	0.06	0.06
Others	0.15	0.15	0.15
Aluminum	Remainder	Remainder	Remainder

An additional solution to the maintenance issues associated with AA7075 is to employ different aluminum alloys. As FTMT and RRA were being explored, new alloys were being developed with more desirable qualities. Two alloys are currently under consideration for AA7075 replacement: AA7150 and AA7249.

As seen in Table 2, the composition of these alloys differs primarily in the concentration of zirconium and chromium. Copper increases the strength; its addition must be limited because it decreases corrosion resistance. Zinc and magnesium together form the strengthening precipitate, $MgZn_2$. The manganese, chromium, and zirconium are added to help control the recrystallization process and to stabilize the grain structure. By doing this, the presence of manganese, chromium, and zirconium help resistance to EAC because it is difficult for cracks to propagate perpendicular the stabilized, elongated grain structure of plate and sheet. Iron, silicon, and titanium are present as impurities. Iron and silicon promote pitting in the alloy because they form constituents that are cathodic. Titanium does not affect the corrosion resistance of aluminum alloys.[21]

Table 3: Mechanical properties of selected 7XXX series alloys

Property	Units	7075	7150	7249
Ultimate Yield Strength	ksi	81	86	83
Tensile Strength	ksi	72	80	76
Compression Yield Strength	ksi	72	79	79
Elongation	%	7.0	8.0	7.0
Toughness	$ksi*in^{1/2}$	12	21	24
Young's Modulus	10^3 ksi	10.4	10.4	10.1
Density	in^3/lb	9.90	9.80	9.80

The first new 7XXX series alloy investigated by the SLAP Program was AA7150-T77. Originally introduced in the 1970's in the T6 temper, AA7150 still had only marginal corrosion resistance, limiting its military applications. The work in both FTMT and RRA proved that the mechanisms for strength and corrosion resistance could be combined to produce more favorable characteristics. Alcoa developed a proprietary process known as the Alcoa 826 Process that resulted in high strength and resistance to EAC. The resulting mechanical properties as seen in Table 3 show that AA7150 meets or exceeds the properties of AA7075-T6. Alcoa produces both plate (T7751) and extrusion products (T77511) from AA7150. Because the process is proprietary, it is difficult for the Navy and Air Force to fully make use of the better qualities of the AA7150. The products are always received in their final form, therefore it is not possible to make adjustments or treat parts after procurement. AA7150-T77 has been used in aircraft since 1987 with its first application being the keel beam on the Boeing 767 aircraft. In 13 years, there have been no EAC issues with the AA7150 in this application.

AA7249 is another alloy under consideration for use in the P-3C and is available only in extrusion form. Table 3 shows that like AA7150, AA7249 meets or exceeds all the mechanical and environmental properties of AA7075-T6 in the T76511 temper. Although the strength of AA7249 is not as great as AA7150, AA7249 can utilize non-proprietary heat treatments. In addition, AA7249 has excellent fracture toughness and corrosion resistance.[22] The combination of the excellent environmental qualities and non-proprietary heat treatment keeps AA7249 an option for military applications such as the P-3C.

Effects of Processing on Aluminum Alloys

Fundamentals of the Extrusion Process

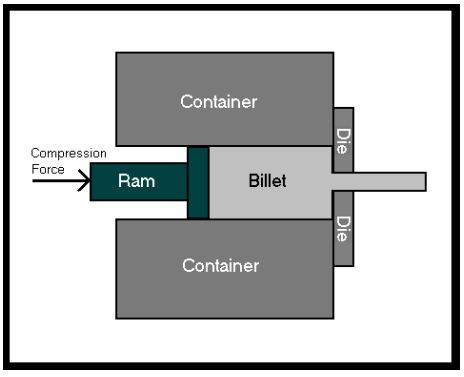

Figure 6: The general extrusion process

Being over 100 years old, the fundamentals of the extrusion process within the aluminum industry have been well developed. Extruded parts are often used in military applications, as in the case with the P-3C. Extruding, similar to cutting, rolling, forging, and drawing, is a manufacturing process. In general, extrusion is forcing a block of metal, referred to as a billet, by compression through an opening that is smaller in cross-section than the original billet.

Figure 6 shows the general extrusion process. As the billet is forced through the die, friction along the walls of the container results in complex grain flow patterns. One way to reduce this friction is to increase the

temperature of the process. Increasing the temperature reduces the flow stress. However, problems can result from this increase in temperature. If the ram is moving too quickly, the local temperatures may be pushed over the melting temperature of the material. In addition, the elevated temperature will cause recrystallization near the surface of the extrusion.[23] Recrystallization is undesirable because it causes a decrease in strength and exfoliation resistance.[24] Often this recrystallized layer can be removed during the final machining of the part.

Extruded parts have good dimensional tolerances. The major drawback of extruding is the requirement of uniform cross-section over the entire length of the part. The process of extruding can be done either hot or cold; a hot extrusion facilitates the necessary deformation and may serve as a heat treatment. Because the extrusion process imparts a great deal of cold work into the material, it is often necessary to either heat treat the material during or after the process in order to eliminate this cold work and optimize properties.

The extrusion ratio, a ratio that compares the original cross-section of the billet to the final cross-section of the extruded piece, can be used to describe several general trends. In general, the lower the extrusion ratio, the larger the grains, which is detrimental to strength and corrosion characteristics. In addition, lower extrusion ratios must be produced more slowly in order to maintain the necessary temperatures. Although it is generally beneficial to produce at the highest extrusion ratio, practical limits are placed on the ratio due to the mechanical limits of machinery. In industry, typical extrusion ratios are between 20 and 30.

For the 7XXX series of aluminum alloys, many of the heat treatments require a solution heat treatment followed by some type of aging. It is preferred that the aging be done after mechanical operations.[25] Dimensional changes, both mechanical (thermal expansion/compression) and metallurgical (microstructural), can result from the aging treatment. Though they may be slight, these changes can be significant to final tolerances. Often a subsequent machining process is done to counter these effects.[26]

Effect of Processing on Microstructure

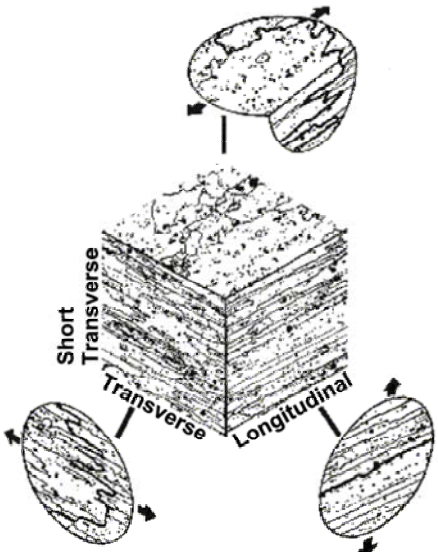

Figure 7: Schematic of grain structure in a plate material

Upon comparison with the grain structure that develops in a rolled plate, the grain shape and orientation observed in an extrusion may vary more significantly from the surface to the center due to the considerable shearing that the metal may undergo near the surface during the extrusion process. In addition, as the extruded part deviates from a simple geometrical cross section such as a bar, the grain flow patterns become more complicated.

In a simple geometry, as in a rolled plate, each face or direction is designated with a particular orientation. Figure 7 shows a typical rolled plate, each face labeled according to its orientation relative to the rolling direction. The direction in which the material is rolled is labeled as the longitudinal (L) direction.[27] It is often characterized by a thin, elongated grain structure in the direction of rolling. Perpendicular to that direction is the long transverse (T)

direction. Grains are elongated in this direction, but not as much as in the L-direction. The TL-plane can be characterized by flat, pancake-like grains. The third direction, perpendicular to the other two directions, is also the cross-section for the plate. This direction is the short transverse direction (S) and the grains are compressed in this direction.

In contrast, the grain structure of a T-shaped extrusion as compared with that of a rolled plate indicates that the directions of longitudinal, long transverse, and short transverse are not fixed to a particular dimension of the component as in a rolled plate, but vary with position within the cross-section of extrusion according to the extrusion geometry and the grain flow that has occurred.

Effects of the Environment on Aluminum Alloys

Stress Corrosion Cracking

Stress corrosion cracking (SCC) is a phenomenon that occurs under a combination of stress and corrosive action. Cracks that propagate under the combination of mechanical stress and corrosion reactions are classified as stress corrosion cracks. Because the environment plays an essential role in stress corrosion cracking, it is also known as environmentally assisted cracking (EAC). Stress corrosion cracks can be virtually invisible except to some non-destructive examinations. This is particularly dangerous when dealing with aircraft because the problem may not be known to exist until after failure has occurred. A number of catastrophic failures in AA7075-T6 have been documented to be a result of SCC.[28] Thus, in recent years, the Navy, along with the Air Force and industry, has devoted resources to develop an understanding of stress corrosion cracking.

Although stress corrosion cracking can be identified and even measured, the underlying mechanisms are not yet fully understood. Although it is generally agreed that electrochemical factors primarily cause stress corrosion cracking, research continues to identify all the factors involved in the phenomenon[29]and to develop test methods that reliably quantify this phenomenon.

Crack Growth Due to Stress Corrosion Cracking

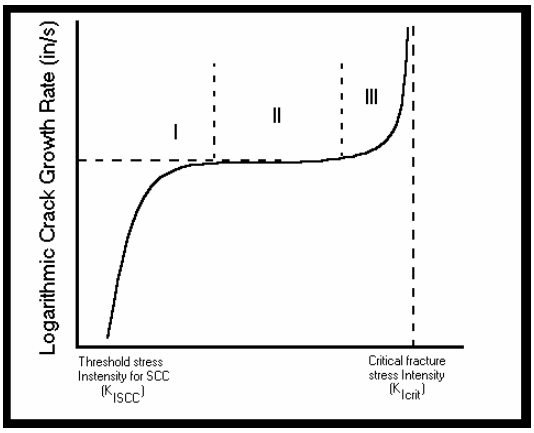

Figure 8: Schematic of the Stages of Stress Corrosion Cracking

Rather than being an instantaneous, catastrophic failure, the process of stress corrosion cracking requires time. Propagating at slow rates (10^{-9} to 10^{-6} m/s), the cracks continue to grow until the stress concentration in the remaining material reaches the critical stress intensity factor, causing fracture. As seen in Figure 8, stress corrosion cracking occurs in three stages. Cracks initiate at surface flaws that can exist because of corrosion, wear, the presence of porosity, or mechanical damage. Several factors affect the crack growth rate, even for the same material. Some of the environmental factors include temperature, pressure,

concentration, pH, electrochemical potential, and stirring or mixing of a corrosive solution. Mechanical factors include the magnitude of the applied stress and the mode of loading on the sample.[30]

In Stage I of propagation, the combination of a stress, usually tensile in nature, and an environment causes the initiation of a stress corrosion crack. The value at which the crack begins to grow is at the stress corrosion cracking critical intensity, K_{ISCC}. This value is determined by several factors including the alloy condition (temper), the environment, and the stress level. The crack growth rate continues to decelerate until it reaches Stage II, steady-state crack propagation. During this stage, the crack tip velocity is limited not by stress, but rather by rate-limiting environmental processes. Some of these factors can be mass transport along the crack to or away from the tip, reaction in the solution, surface reactions on the material, or hydrogen absorption into the bulk.[31] In Stage III, the crack has reached a length for which the stress intensity factor approaches the critical stress intensity factor, K_{Icrit}, which describes at what point the material would fail mechanically in an inert environment. Once the stress intensity factor reaches this critical stress intensity factor, K_{Icrit}, the material fails catastrophically. Environmental testing technique in this work quantifies the Stage II crack growth rate for comparison to AA7075-T6. It is this crack growth rate that determines the time it will take for a stress corrosion crack to reach a catastrophic length and cause failure.

Stress Corrosion Cracking Mechanisms

In 1940, the electrochemical theory of stress corrosion cracking was developed.[32] Since then, several other theories have been developed, most of them using either cathodic or anodic reactions as the primary mechanism of stress corrosion cracking in aluminum. One reason that it is so difficult to determine the mechanisms for stress corrosion cracking is because it is difficult to identify where crack initiation begins; it is difficult to distinguish pitting or intergranular corrosion from true crack initiation.

Aluminum is a thermodynamically active material, second only to beryllium and magnesium. The reason that aluminum is generally effective in resisting corrosion is because it forms a protective oxide film barrier that is strongly bonded to its surface. The oxide film, which forms in normal atmosphere, is thermodynamically stable over a range of pH from 4 to 8.5. Outside of this limit, its oxides are reactive with acids and bases, thus sacrificing its protective barrier.[33] In addition to this barrier, the composition of the solid solution as well as the amount, size, and location of other phases within the alloy have an effect on corrosion behavior. The second-phase precipitates often have a different electrochemical potential than the solid solution aluminum matrix, thus creating localized galvanic cells.

Stress corrosion cracking in the 7XXX series aluminum alloys tends to be the most damaging type of corrosion when compared to pitting and general corrosion because it involves intergranular cracking. Intergranular cracking can occur due to phases along the grain boundaries that are anodic compared to the remainder of the microstructure. Therefore, the location of the second phase can play a large role in stress corrosion cracking. The primary precipitate in AA7075 is $MgZn_2$. In the T6 temper, the $MgZn_2$ is precipitated along the grain boundaries as η'. In the T7X temper, the η precipitates dispersed along the grain boundaries are fewer in number but larger in size. In the T6 condition, the numerous η form galvanic cells with the rest of the matrix, which may create the environment required for stress corrosion cracking.

Regardless of the exact failure mechanism, failure occurs via an intergranular fracture mode that results in a strong dependence on the grain structure.

Method of Investigation

Purpose

The grain flow patterns that develop in extruded aluminum parts are important in terms of predicting a components resistance to EAC phenomena while in service. The effect of grain structure and orientation relative to the direction of applied tensile stress in aluminum alloys and tempers that are susceptible to environmentally assisted cracking is well known. In plate materials, the enhanced susceptibility of AA7075 to EAC when stressed in the ST direction compared to the L or T directions has been documented in the laboratory as well as in the field. In addition, it has been documented that as a grain structure becomes more uniform and equiaxed, or rounded, the degradation in EAC resistance for a specimen stressed in the T direction far exceeds the improvement observed in the ST orientation.[34] The magnitudes of these effects are dependent upon alloy, temper and environment. One may expect that in an extrusion, the orientation dependence of EAC resistance is fixed to the grain flow pattern rather that the part itself. Therefore, the grain flow pattern in an extrusion must be considered in conjunction with the primary loading directions for the structure of interest.

Material

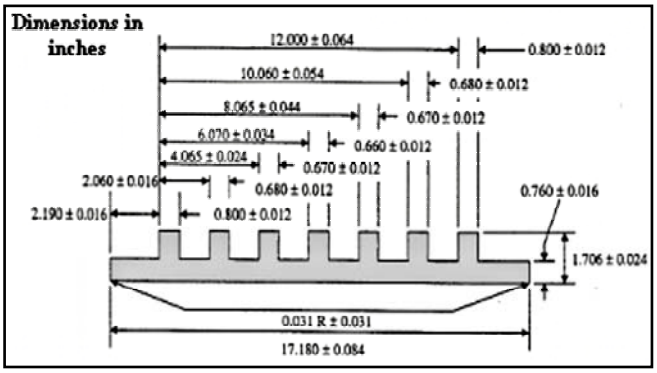

Figure 9: Cross-section of wide panel extrusion

In order to determine the effect of processing on the EAC characteristics, both mechanical and environmental tests were conducted on two extrusion types. Figure 9 shows the cross-section of an AA7249-T76511 wide panel extrusion that forms part of the outer wing section of the P-3C. For comparison purposes, an additional AA7249-T76511 extrusion was obtained with a cross section (perpendicular to the extruded direction) of 2 x 3-in. (2.5 x 7.6-cm). This simple extrusion was intended as a baseline against which the more complicated wide panel extrusion would be compared. The extrusion ratio of this plate was about 6.5 and that of the wide panel extrusion was approximately 25.

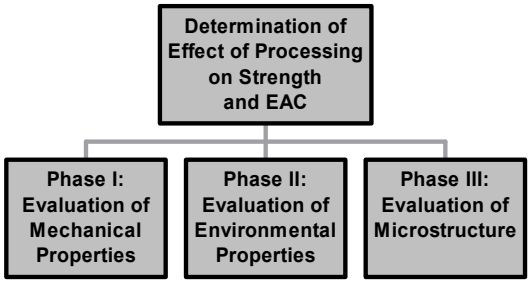

Figure 10: Organization of Experimental Procedure

Experimental Procedure

The project was divided into three different phases as seen in Figure 10. Each phase concentrates on a different aspect of the research. Phase I of this study involved a characterization of local properties such as electrical conductivity, hardness, and strength as a function of position within the extrusion. Phase II focused on characterizing the EAC properties of the

alloy. Running concurrent with both Phase I and Phase II of this study was Phase III, which served several different purposes. During Phase III, a microscopic examination documented grain orientation and flow pattern as a function of position in the extrusion in all planes. This information was used to determine the specimen removal locations and orientations that were used in EAC testing. Optical microscopy was also used to characterize grain flow patterns in selected samples and to help quantify the extent of the impact of the environment. In addition, fracture surfaces were observed on the SEM to determine the extent of brittle and ductile fracture.

Test Methods

Phase I: Evaluation of Mechanical Properties

Hardness Measurements

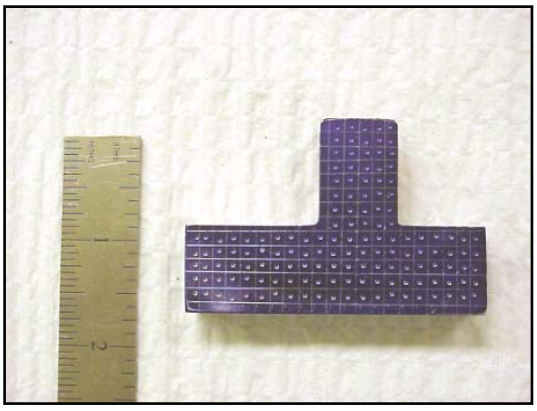

Figure 11: Wide panel extrusion hardness specimen

Hardness testing provides a comparative measure of a material's resistance to indentation and permanent deformation. These results can be directly correlated to tensile strength. As a possible way to determine the difference in strength along the extrusions, the cross-sectional area perpendicular to the direction of extrusion was taken from each extrusion and divided into approximately 1/8-in squares. In the center of each square, a hardness measurement was made. The resulting measurements were plotted on a contour map to determine if variations existed. The wide panel was divided into seven sections, each containing a riser. Figure 11 shows the hardness measurements taken on one of the wide panel extrusion sections. Measurements were taken in a similar manner across the entire cross-section of the 2-inch extrusion. The face shown in Figure 11 was the focus of these measurements because the most variation in microstructure occurred in this direction.

Tensile Testing

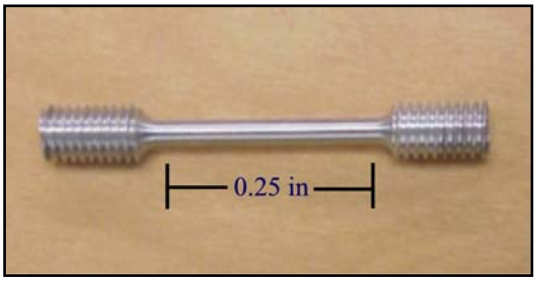

Figure 12: Sub-sized tensile specimen

Tensile testing provides a measure of strength, ductility, and stiffness. Testing was performed in accordance with ASTM standard B557-94.[35] After completing hardness maps of both extrusions and some preliminary optical microscopy, locations for specimen removal were selected from both extrusions. Several locations were selected for each specimen. At each location, three sub-sized specimen were taken to provide a method of validation of results. Figure 12 shows a sub-sized tensile specimen.

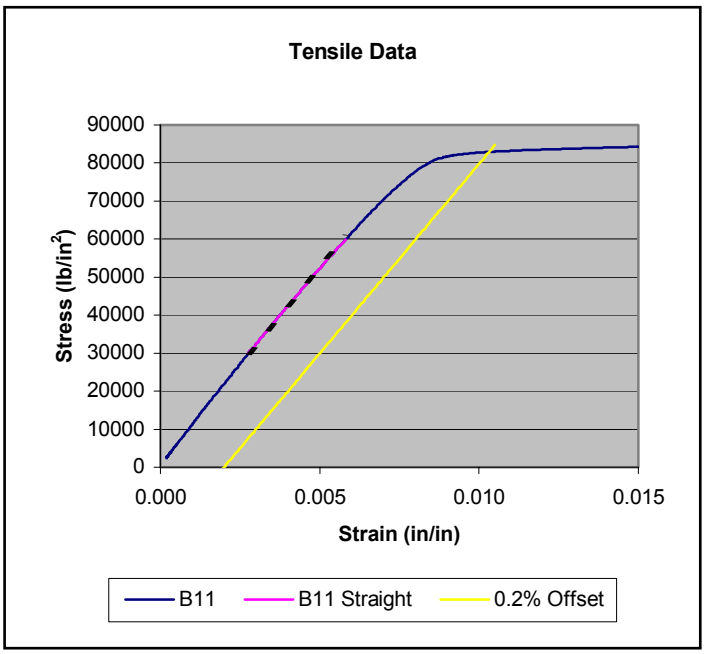

Figure 13: Sample tensile data

Analysis of tensile data provides several mechanical properties. Figure 13 illustrates typical tensile results for an aluminum sample. Tensile testing is designed primarily to provide a measure of strength. From the data, two types of strength can be determined. The first type of strength is called yield strength (YTS). For aluminum, yield strength is determined by finding the intersection between the data and the 0.2% offset line. The slope of this line is determined by finding the slope of the straight-line portion of the data. The x-intersect of the line is then set at 0.2% strain. Yield strength determines the maximum stress for the material where the deformation remains elastic. After this stress, the material plastically deforms.

The other type of strength drawn from the data is ultimate tensile strength (UTS), which describes the maximum stress that a material can withstand. This is often characterized in ductile materials such as aluminum by severe localized deformation called necking. Though ultimate tensile strength is relatively unimportant in materials selection because yield strength predicts deformation, it is often reported in materials handbooks because it provides a quantitative comparison among materials.[36]

In addition to strength, both ductility and stiffness can be determined from the tensile data. The slope of the straight portion of the data is called Young's modulus or the modulus of elasticity. Stiffness between materials can be compared for materials selection depending on the application. If a material is required to handle large stresses without deforming, a stiffer material with a steeper slope is selected. Ductility is a quantification of the amount of deformation a specimen can withstand before breaking and can be measured in one of two ways: as a percent elongation or a percent reduction in area. Ductility is important in both fabrication and application. During fabrication, some ductility is desired so that the material can be formed without breaking the material. In application, some ductility is desired so that deformation occurs before yielding if the applied stress is too high.[37]

Conductivity Measurements

Although conductivity testing is not a mechanical test, conductivity measurements have been used as a non-destructive indication of EAC resistance within an alloy system. Therefore, prior to any destructive tests, conductivity measurements were made in several locations for each of the specimen. This testing was performed using a commercially available eddy current system calibrated with standard specimens according to ASTM standard E1004-99[38]. Each measurement from the conductivity probe averages a reading over a diameter of 0.4-in. (1.0-cm),

limiting the mapping capability of this parameter. In order to have some possible correlation between the properties and position, conductivity measurements were taken where tensile specimens were drawn from the extrusions.

Phase II: Evaluation of Environmental Properties

Double Cantilever Beam

Figure 14: Double cantilever beam specimen

Double cantilever beam (DCB) testing, performed in accordance with ASTM practice G 168-00,[39] provides a method to measure the rate of environmentally assisted crack rate propagation. DCB specimens were taken from each of the three extrusions. All of the specimens were loaded in the short transverse direction, the most susceptible direction to stress corrosion cracking. The specimens were notched and then precracked using a fatigue precracking method. The precracking and loading procedure are detailed in Appendix B. Figure 14 shows a DCB specimen as measured.

The crack growth rate is a function of the applied stress intensity factor as shown in Figure 15. Upon loading a DCB specimen as described in Appendix B, the test begins near the critical stress intensity factor (K_{Icrit}) and travels down the curve. Because the bolts are not adjusted over the course of the test, the crack mouth opening displacement remains constant. As a result, as the crack grows, the load actually placed on the specimen decreases, resulting in a decreasing stress intensity factor. In this study, the double cantilever beam tests were used to quantify the Stage II EAC propagation rates for this alloy, and were not used to obtain the entire curve shown in Figure 15 .

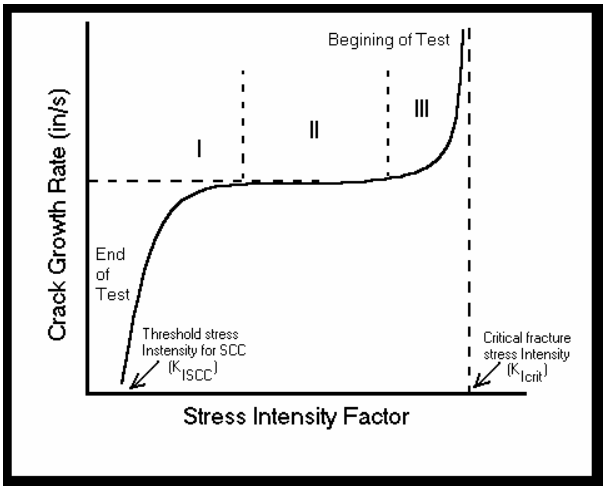

Figure 15: Stress corrosion crack growth rate in DCB specimen

Slow Strain Rate Testing

Slow strain rate testing (SSRT) was the other type of environmental testing employed in this study and was performed in accordance with ASTM standard G129-95.[40] This testing differs from double cantilever beam testing in that it provides a means to observe and measure crack initiation and propagation versus solely crack propagation. SSRT uses the same sub-sized specimen used in tensile testing. Instead of pulling quickly until fracture as in a tensile test, slow strain rate tests pull at a much slower rate (10^{-4} to 10^{-8} in/s), slow enough for the environment to interact with the sample. Typically, the results from the slow strain rate tests in a test environment are compared to a slow strain rate test in an ambient environment. The susceptibility to EAC is then determined by comparing the behavior in both environments.[41] This allows investigation of EAC as a function of location within the extrusion. Figure 16 shows a slow strain rate test set up immersed in the salt-water environment. The procedure followed for the SSRT is detailed in Appendix E.

Figure 16: Slow strain rate test rig with specimen immersed in NaCl solution.

Slow strain rate testing has been recently developed as an alternative to alternate immersion testing. Alternate immersion testing immerses a stressed specimen for 10 minutes out of every hour and then measures time to failure. Not only is there significant scatter in the data, but also it is time consuming. Previous testing has shown that average stress corrosion cracks grow at a rate of 10^{-6} to 10^{-9} m/s, which would fail in a few days.[42] However, crack initiation often requires a long amount of time. As a result, slow strain rate testing has been developed to produce more reliable results in a shorter time to compare the susceptibility to stress corrosion cracking. Another advantage is that the specimens are small and can be removed from different areas of the microstructures.

Slow strain rate testing was conducted in two environments: an ambient environment (laboratory air) and a test environment (1.0 M NaCl). Similar specimens, taken from similar locations in the extrusion, were tested in both environments. Specimens were taken from the L and ST direction from both the 2-inch and wide panel extrusion. The L direction was chosen in order to have some basis for comparison with the tensile tests that were run. However, specimens from the ST direction were also run, as this direction is traditionally the most susceptible to stress corrosion cracking. As testing was completed, it was necessary to describe the microstructures from which way it was extracted. Due to the complex grain flow in extrusions, particularly the wide panel extrusion, it is difficult to maintain consistent names. Microstructures, detailed in the following sections, are best described by the shape and orientation of the grains.

Phase III: Microscopy

Optical Microscopy

Optical microscopy was conducted to document the grain orientation and flow pattern as a function of position for each of the three extrusions. Each extrusion was sectioned into symmetrical parts. At least one of those symmetric parts was polished using traditional metallographic preparation. Each section was then etched using Keller's reagent to reveal the grain structure. The Nikon Epiphot 200 Optical Microscope was used to obtain optical images of the material microstructures.

Fractography

After fracture of a slow strain rate specimen, the specimen was cleaned in acetone followed by alcohol. The specimens were then preserved in a dessicator until analyzed. The fracture surfaces of the smaller end of the broken specimen were put into the SEM and analyzed at low (approximately 80x) and high (approximately 1000x) magnification. Low magnification was used for several analyses: calculation of the total area for reduction in area, identification and quantification of brittle and ductile areas, and identification of possible initiation sites. High magnification was used as a verification of the trends and quantities observed in low magnification. As seen in Figure 17, an SEM fractograph taken at 1027 times magnification, ductile areas are characterized by the presence of large ridges and valleys, whereas brittle areas are flatter and smoother.

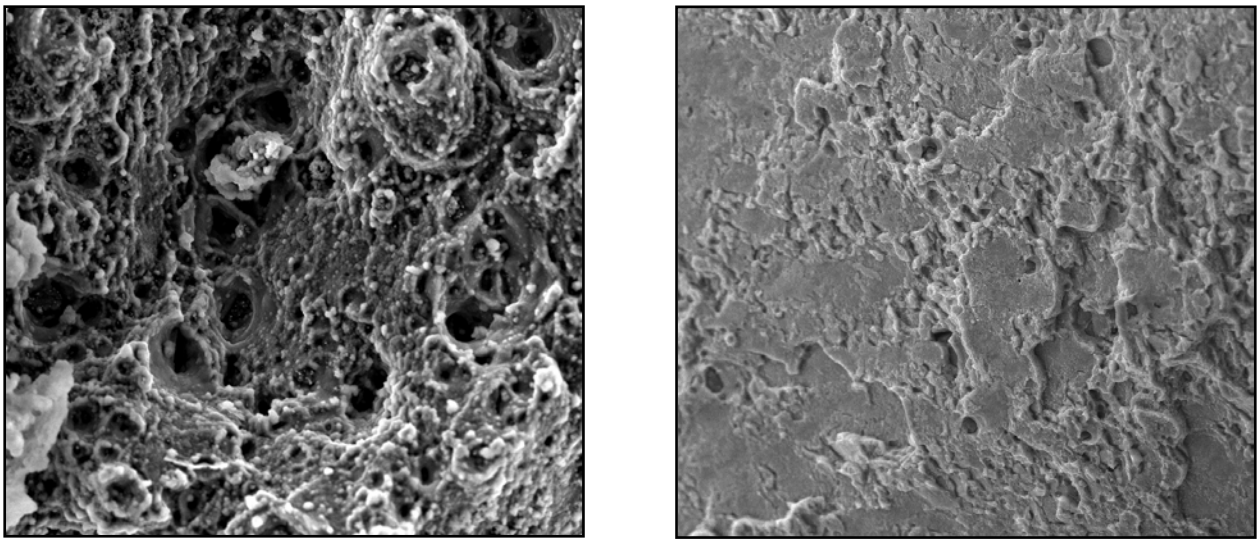

Figure 17: Examples of ductile (left) and brittle (right) surfaces as observed in the SEM (x1000)

Cross-sectioning

Cross-sectioning was used as an additional method to quantify the susceptibility to stress corrosion cracking qualitatively. The longer end of the broken slow strain rate specimen was sectioned through the middle plane, mounted, and polished using traditional metallographic preparation. The section was then etched using Keller's reagent to reveal where stress corrosion damage was located within the grain structure.

Results

Initial Optical Microscopy

Microstructural characterization of the grain structure on three orthogonal planes was conducted as a function of position within the extrusions. Because the microstructure of the wide panel extrusion was expected to vary from that of a plate, the traditional labels for planes with respect to the extruded direction (longitudinal) were replaced. Instead of these grain structures being fixed to a specific plane, they changed as the grain flow changed as a result of the extrusion process. Three new labels were defined for each face or plane of the plate: "E", "P", and "O". The "E" face refers to the plane that contains the direction of extrusion and the short direction. In a plate, this plane would be referred to as the LS plane and is typically characterized by elongated grains. The "P" plane is the plane that contains the extrusion direction and the long transverse direction. Grains in this plane are typically flat and somewhat elongated. The final face, the "O" plane, is orthogonal to both the E and P planes. Its grains can be equiaxed or elongated depending on the processing of the material.

Both extrusions were sectioned to reveal each of the three planes and prepared to characterize the grain flow and orientation. The 2-inch extrusion, expected to be plate-like in its microstructure, was used as a control for comparison to the WP extrusion. Once sectioned, the 2-inch plate revealed some differences in grain flow and structure compared to what is traditionally observed in a plate.

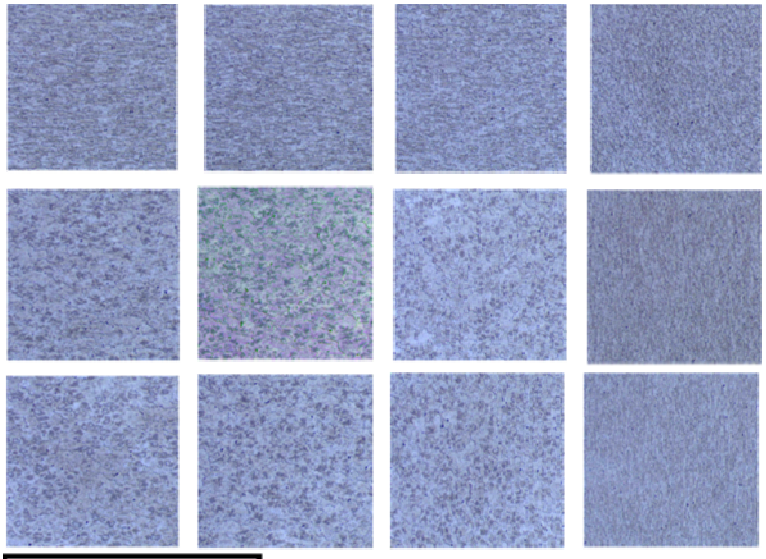

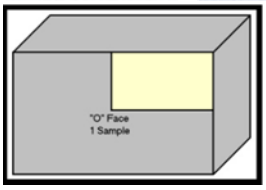

Figure 18: Optical microscopy revealing the grain flow and orientation of the 2-inch extrusion (x100)

Inset: Location of sample taken for optical microscopy in relation to extrusion

Figure 18 is a section removed from the 2-inch extrusion for optical microscopy. A quarter of the sample is shown, as the remainder of the face is symmetrical. Rather than a uniform cross-section showing grains of similar size and orientation, the microscopy reveals that on the edges of the extrusion, the grains are elongated in a direction parallel to the edges. In the corners, the grains are much finer than in the middle, where the grains are much more equiaxed and larger in size. These characteristics result from the extrusion process. As the billet is pushed through the die, the sides of the extrusion are subject to more friction whereas the material flows more readily through the middle, resulting in the grain structure seen in the 2-inch extrusion.

The wide panel extrusion was sectioned in the same manner as the 2-inch extrusion. Several risers were examined for the grain flow and orientation to determine if the entire cross-

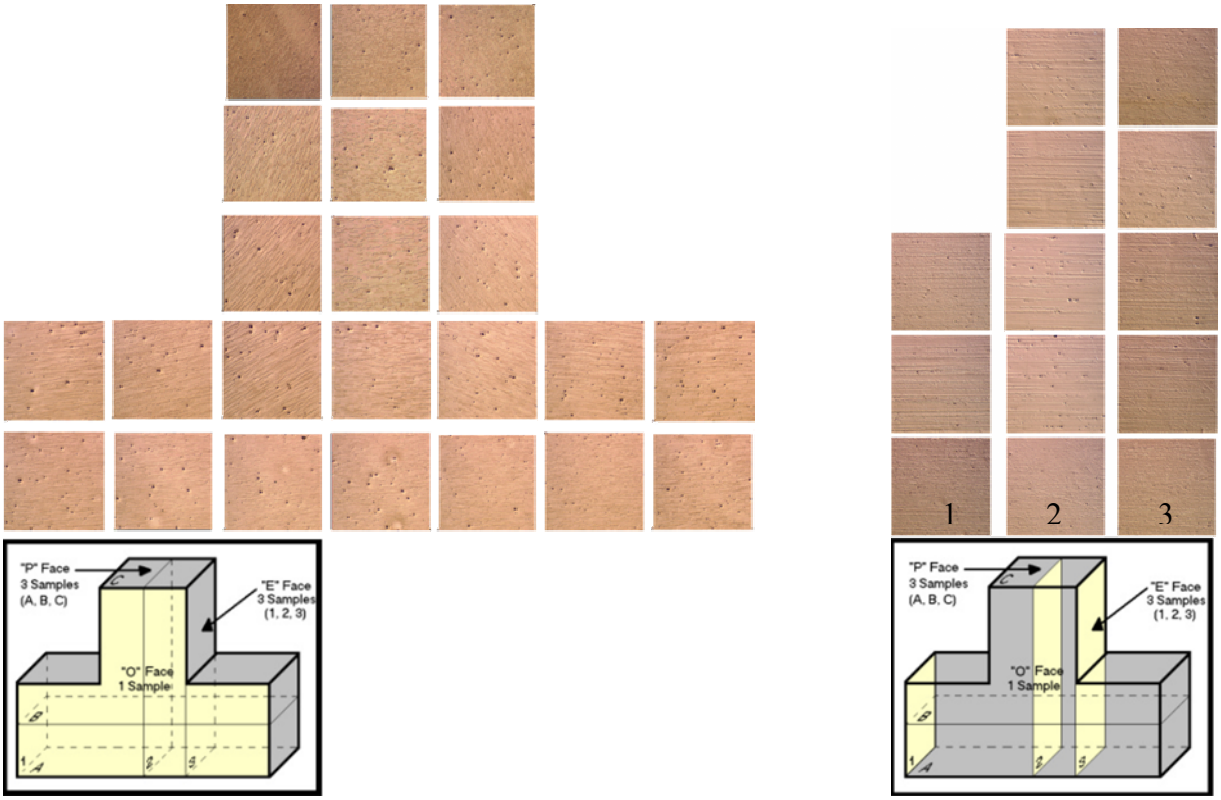

Figure 19: Optical microscopy revealing the grain flow and orientation of the wide panel extrusion. Each face of micrographs is accompanied by a diagram detailing where the faces were taken from on the extrusion. The top left picture is the O face; the top right is the E face, and the bottom left is the P face. (x100)

section was uniform. The top left picture in Figure 19 shows the resulting microstructure that is representative of the entire cross-section (O face). The metallography indicates that the grain flow is more "plate-like," or elongated in the T direction, in the regions in between the risers and that the orientation of the elongated direction of the grains changes by more than 45 degrees at the corners of the risers. The grains become more elongated on the O face as the distance from

the top of the extrusion increases, both under the riser and in-between risers. In addition, the grain structure is more equiaxed at the center of the riser.

The optical microscopies for the other two faces are also shown in Figure 19. The E face, represented in the top right corner, is uniform through the extrusion as seen in sections 1, 2, and 3; all the grains are elongated as expected in the extruded direction. Conversely, the P direction had a significant amount of variation depending on the location in the extrusion. Towards the middle of the extrusion (plane B), the grains are flat and elongated as expected. However, at the ends of the extrusion (plane A and C), the grains are not as flat, but elongated and finer. As in the O face, this is a result of the extrusion process. As aluminum is forced through the die, the grains on the outside see more cold work and thus have a different structure than those in the middle.

The results from the microscopy were combined with the results from the mechanical tests to determine the location from which specimen were removed for the slow strain rate testing.

Phase I: Mechanical Results

Hardness Measurements

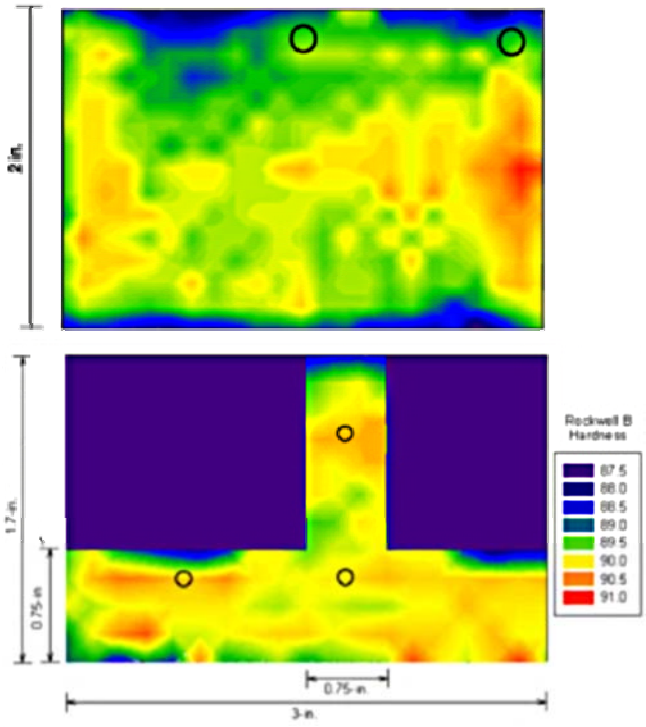

Figure 20: Contour plots of hardness measurements

Figure 20 shows the results from the hardness measurements taken on both the 2-inch and wide panel extrusion. Results indicate that overall, the Rockwell B (R_B) hardness variation on the cross section perpendicular to the extrusion direction is minimal. This is not surprising since the heat treatment conducted subsequent to the extrusion process likely eliminated any variations in strength due to cold work. However, slightly softer spots are indicated near the top and bottom of the 2-inch thick extrusions.

In addition, local soft areas are noted between the risers and at the riser edge in the wide panel extrusion. This phenomenon was observed at multiple riser locations. Average quantities indicate that the 2-inch (5.1-cm) thick extrusion ($R_B = 90.4 \pm 0.4$) is slightly harder than the wide panel extrusion with an overall average value of $R_B = 89.3 \pm 0.8$.

Tensile specimens were chosen from the E face for both the wide panel and the 2-inch extrusion as typical tensile tests are run in the L-direction. The circles on Figure 20 represent the area that the tensile specimens were drawn. Three specimens were drawn in each location and

tested. The locations were chosen primarily using the optical microscopy results, as the hardness measurements did not show significant variation.

Tensile Testing

Tensile testing on 20 specimens was completed. Details of the testing and analysis procedure are included in Appendix C. The results, combined with the results from the other mechanical measurements are combined in Figure 21.

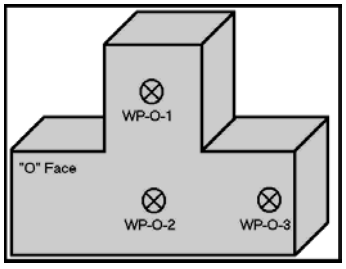

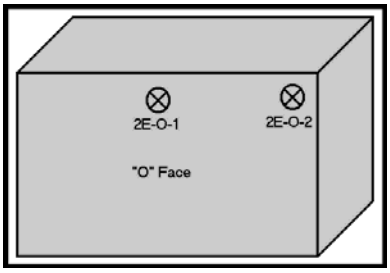

2-inch Extrusion		Corner 2E-O-1	Top Center 2E-O-2	Whole Piece
Conductivity	%IACS	37.8	37.8	37.7
Hardness	HRB	90.4	90.3	90.4
YTS	ksi	81.95	83.68	82.82
UTS	ksi	86.81	81.95	87.33
Modulus	10^3 ksi	9.70	9.84	9.77

Wide Panel		Top of Riser WP-O-1	Bottom of Riser WP-O-2	Between Riser WP-O-3	Whole Piece
Conductivity	%IACS	38.8	38.6	38.4	38.5
Hardness	HRB	88.8	89.6	89.2	89.3
YTS	ksi	80.44	79.43	78.24	79.26
UTS	ksi	85.70	85.01	82.72	84.40
Modulus	10^3 ksi	9.72	9.61	9.58	9.62

Figure 21: Summary of mechanical test results

The results show further that there is no mechanical variation in the extrusion. The variation between the areas is minimal, although the 2-inch extrusion tends to be slightly stronger.

Conductivity Measurements

Conductivity measurements were obtained for the 2-inch and wide panel extrusion; the average values were 37.7 ± 0.1 and 38.4 ± 0.2 % IACS [(1)], respectively. The similar values obtained for

[1] %IACS (% international annealed copper standard) refers to a percentage of the conductivity of annealed copper.

both extrusions indicate that amount of aging obtained in each T76511 extrusion is similar since the conductivity of these alloys directly correlates with depletion of alloying elements from solid solution[43]. These values are consistent with the range of values obtained from the literature for various tempers of AA7249[44]. The large sampling area of the conductivity probe precluded detailed conductivity maps. However, statistically significant lower conductivity values were measured at the center of the risers compared to locations remote from the risers in the wide panel extrusion.

Phase II: Environmental Results

Double Cantilever Beam Testing

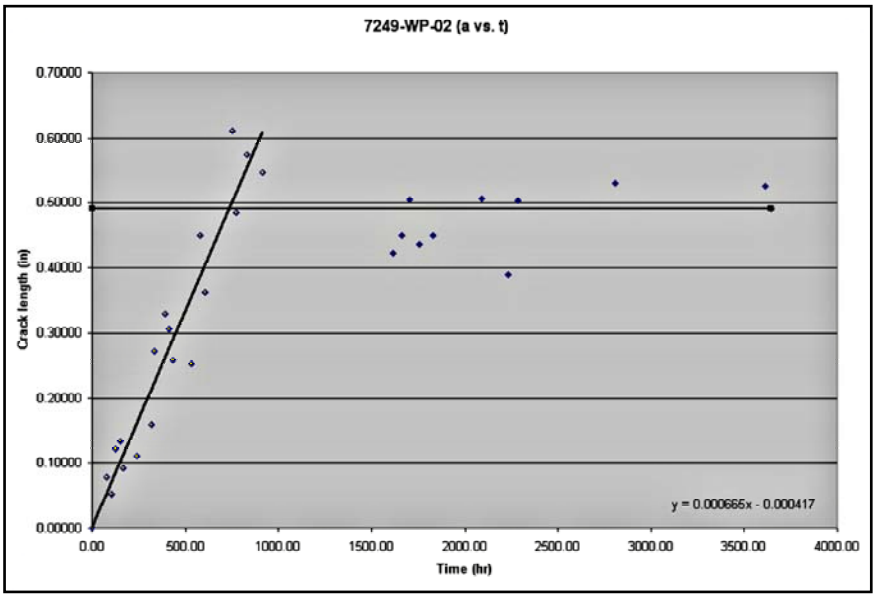

Figure 22: Crack growth rate vs. time for wide panel DCB specimen loaded in the ST direction.

Six specimens were used to determine the effects of the environment on SCC propagation. Each of these specimens has data that is split into two distinct parts: steady state crack growth and crack growth arrest. Figure 22 shows an example of the data drawn from one of the wide panel specimen stressed in the ST direction. The data until about 750 hours represents the steady state crack growth rate. After this point, the data shows that the crack was no longer growing. The final crack length was measured after the specimens were broken open for observation. The length of the crack at this point represents the final crack length. The complete data sets are shown in Appendix D.

Three samples from each extrusion were tested. Each specimen was stressed in the ST direction to 90% of the $K_{I,crit}$ value for AA7249. The specimens were then exposed to a few drops of 0.6 M NaCl on a daily basis. The crack length versus time plot was determined for each specimen in order to identify the straight-line portion of the data to determine the average crack growth rate during the steady crack growth phase of SCC. The resulting values for the average steady state crack growth rate are shown in Table 4. First, the occurrence of crack growth indicated that AA7249 is susceptible to SCC. The results show that the 2-inch extrusion had average crack growth rates much lower than the average crack growth rate for the wide panel extrusion. These results indicate that once

Table 4: Average steady state crack growth rates (in/s) for AA7249 in 2-inch and wide panel extrusion

	2-inch	Wide Panel
Sample 1	1.770E-04	6.650E-04
Sample 2	1.300E-04	4.570E-04
Sample 3	1.410E-04	5.250E-04
Average	1.493E-04	5.490E-04

stress corrosion cracking began in the wide panel extrusion, it would approach the K_{ISCC} value over three times faster than the 2-inch extrusion resulting in an earlier failure.

Upon comparison with AA7075 conditions from a previous study,[45,46] results indicated that the AA7249-76511 extrusions represent an improvement in EAC crack growth resistance over the peak aged condition of AA7075 (T6), but may not represent an improvement over the overaged condition of AA7075 (T7351). However, recall that the overaged condition of AA7075 represents a lower strength condition compared to AA7075-T6 and AA7249-T76511. Figure 23 shows a comparison between AA7075, AA7150, and AA7249.

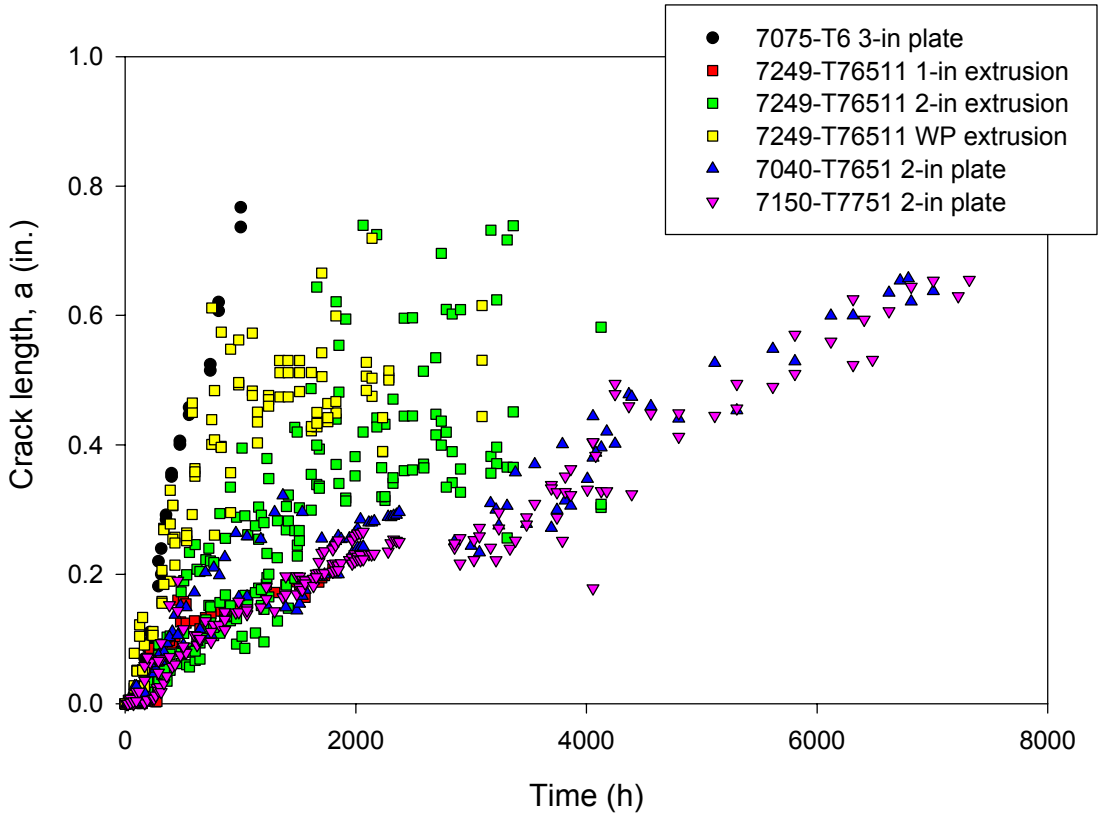

Figure 23: Crack growth versus time for different extrusions from AA7075, AA7150, and AA7249

Slow Strain Rate Testing

Slow strain rate testing was conducted on both the 2-inch and wide panel (WP) extrusion on samples from two different directions. Each orientation for both extrusions had at least four samples run, two in laboratory air and two in 1.0 M NaCl. The applied stress was along the long axis of the specimen blanks shown in Figure 24. Next to each location is a list of the specimens drawn from that location.

2-inch Extrusion

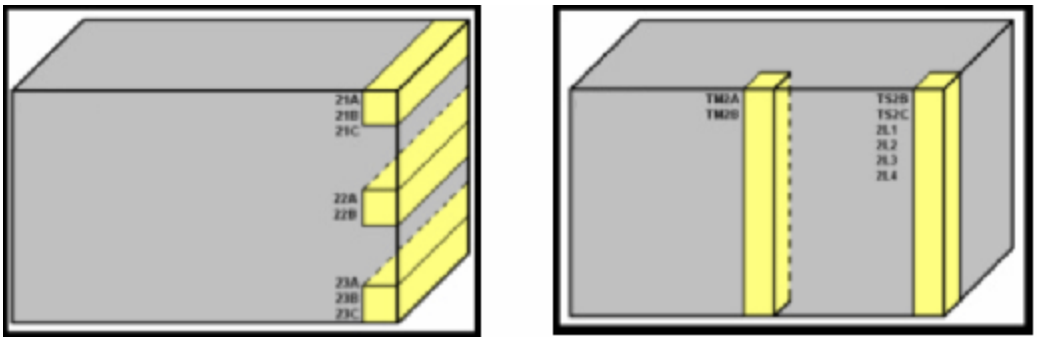

Figure 24: Location of specimen removal for the 2-inch extrusion.

Multiple methods were used to show the susceptibility of the alloy in different orientations. As an initial screening, the reduction in cross-sectional area (RA) at fracture for laboratory air was compared to that in the salt-water solution. Table 5 is an average of all of the specimens for each orientation. As seen by the data, EAC susceptibility is indicated by a larger RA for specimens tested in air than in saltwater. The data also indicates that there is a greater EAC susceptibility when the stress is applied perpendicular to the P plane versus when the stress is applied perpendicular to the O plane and indicated by the larger decrease in RA for the specimens stressed perpendicular to the P plane.

Extrusion	Stress Perpendicular to Plane	Reduction in Area Air	Reduction in Area Salt
2-inch	P	34.15%	29.07%
2-inch	O	30.71%	30.39%

Table 5: Average reduction for 2-inch specimens in air and salt water solution

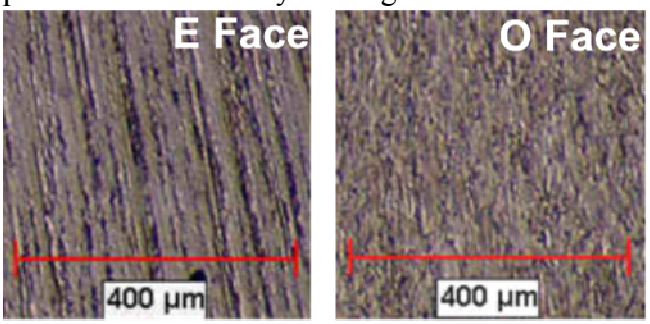

Figure 25: Microstructures of representative specimen from the O and E face of the 2-inch extrusion (x100)

For the 2-inch extrusion, the microstructures of the samples were consistent with the location from which they were extracted. Although the initial microscopy showed differences in the microstructure from the middle of the O plane to the ends of the O plane (Figure 18), the grain structure was similar, particularly when contrasting this structure with the highly elongated structure observed in the E

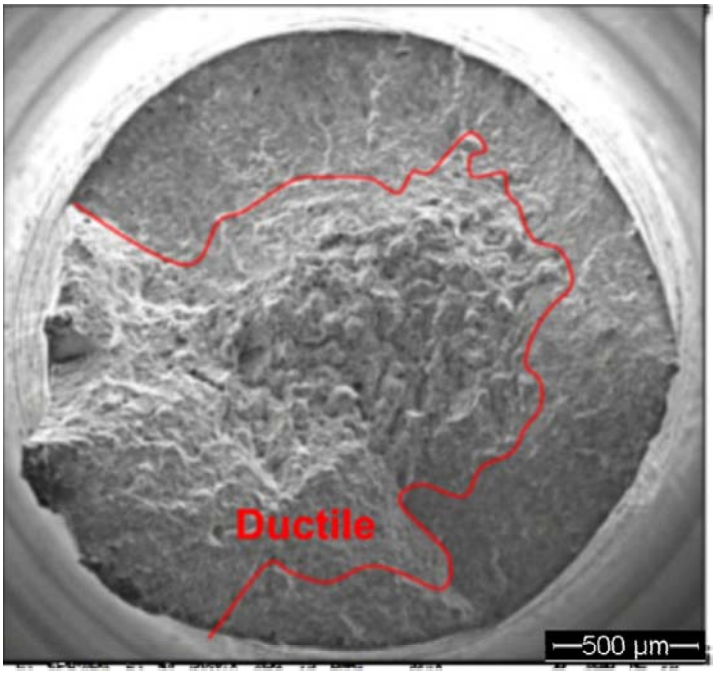

Figure 26: Specimens from 2-inch extrusion stressed perpendicular to the O face in laboratory air (23A, above) and 1.0 M NaCl (23C, below) [77x].

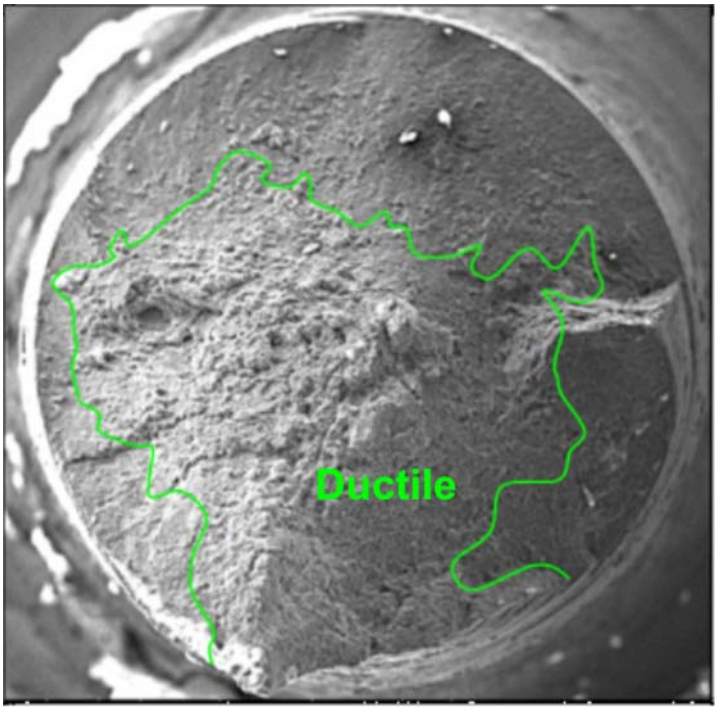

plane (Figure 25).

Fractography was conducted to verify the quantitative data above and the presence of an environment-affected fracture mode. Figures 26 and 27 show the fracture surfaces for a representative specimen from the 2-inch extrusion. Figure 26 shows the specimen stressed perpendicular to the O plane. As seen in a typical tensile test, these specimens fail ultimately from mechanical overload. Ductility is quantified by examining the specimen under high magnification and determining which areas show a great amount of texture or ductility. In the laboratory air specimen (top), the area enclosed by the red line shows the ductile portion of the failure. This area constituted 52% of the total fracture area.

Figure 26 (bottom) shows a fracture surface of a specimen with the same orientation as above, but tested in 1.0 M NaCl. There are two important observations to note. First, the ductile areas on the specimen appear less deformed when observed in higher magnification. The brittle areas appear flatter and less textured in these areas. Secondly, the amount of ductility has decreased in the specimen as estimated by determining the area enclosed by the green perimeter. In this specimen, as compared to the air specimen, ductility has reduced to approximately 49% of the total fracture area. The decrease in ductile fracture area when comparing an air test to a salt-water test is an indication of susceptibility to EAC.

The specimens stressed perpendicular to the P plane were also observed using the SEM microscope. The fracture surfaces, seen in Figure 27, also highlight the brittle and ductile areas. Once again, the specimen run in laboratory air, as seen in the top figure, showed a large ductile area that constituted 59% of

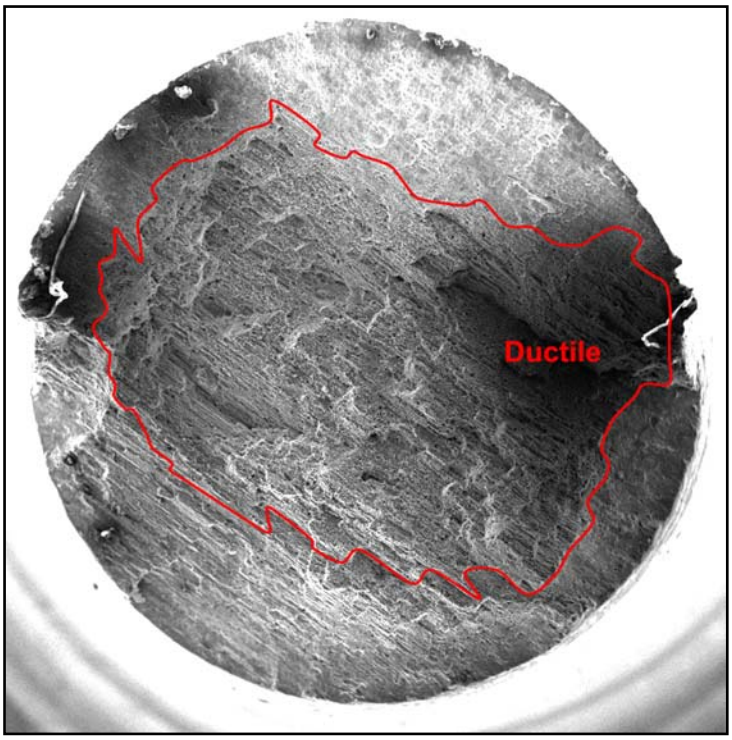

Figure 27: Specimens from 2-inch extrusion stressed perpendicular to the P face in laboratory air (TMRA, above) and 1.0 M NaCl (TMRB, below) [77x].

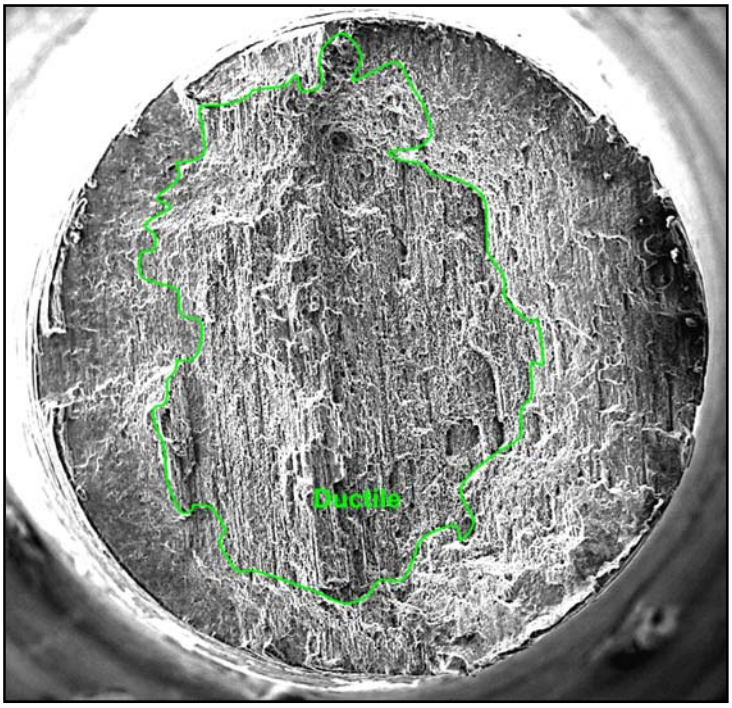

the fracture area. Following the same trend as above, a specimen with the same orientation, but tested in 1.0 M NaCl solution showed a reduction of ductile fracture area; only 50% of the surface was ductile fracture.

It is also observed that the fracture surfaces of the specimens stressed perpendicular to the P plane are less textured in appearance than those stressed perpendicular to the O plane. This is due to the orientation of the microstructure relative to the stressing direction. Whereas the fracture surfaces represent a crack path along the ends of elongated grains for specimens stressed perpendicular to the O plane, the specimens stressed perpendicular to the P plane result in a fracture surface that travels along the elongated grain boundaries.

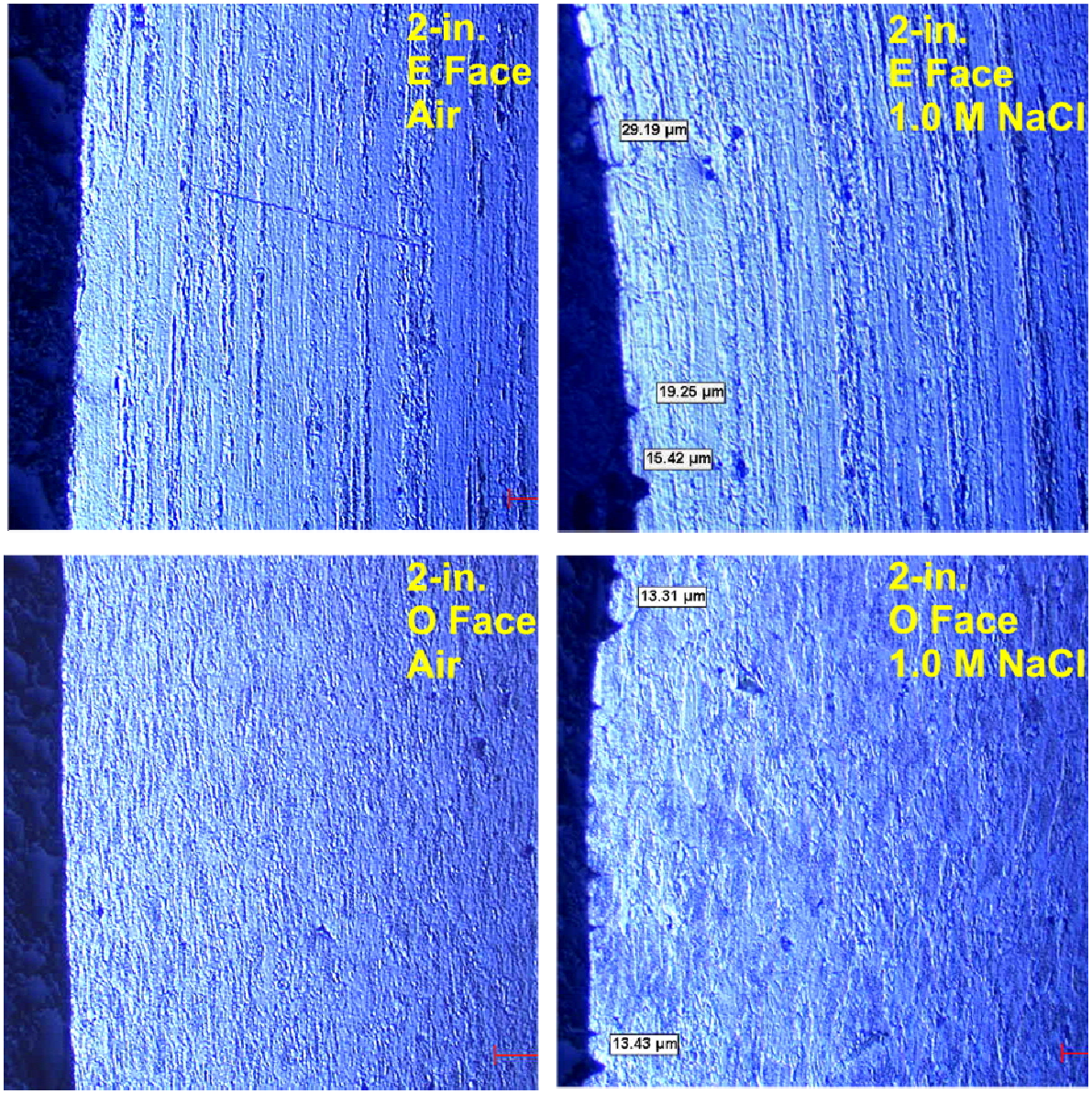

Figure 28: Cross-sections of 2-inch extrusion specimens stressed perpendicular to the O face (23A and 23C, above) and P face (TMRA and TMRB, below) in laboratory air and 1.0 M NaCl (x200).

As an additional validation of these findings, specimens were examined to determine if there was evidence of the beginning of EAC at locations along the gage length away from the fracture surface. One half of each specimen was cross-sectioned and examined metallographically. Figure 28 shows the cross-sections from specimens stressed perpendicular to the O plane (above) and P plane (below) in air and salt water (note the different microstructures). Sectioning shows how the corrosion damage obtained in salt water, visible along the specimen edges as V-shaped notches, occurs at the grain boundaries. In addition, the amount of damage observed along the specimen edge is larger in the specimens stressed perpendicular to the P plane compared to the specimens stressed perpendicular to the O plane. This is due to the

orientation of the elongated grain direction relative to the stress direction and a larger number of grain boundaries intersecting with the specimen surface.

Wide Panel Extrusion

Figure 29 shows the location of the specimens drawn from the wide panel extrusion. Figure 30 shows the RA measurements for the WP slow strain rate tests. These results indicate that specimens stressed perpendicular to the O plane are more ductile if removed from the center of the riser (MR) as compared to in-between the risers (SP). It appears that the different microstructures that may be present on the P planes of these specimens (MR3, MR4, MR5) do not drastically affect ductility or EAC susceptibility. However, a decrease in RA for the salt-water tests indicates that these specimens are susceptible to EAC. Specimens stressed perpendicular to the P plane indicate a large variation in ductility. The specimens removed from the center of the riser (TMRA/B) indicate susceptibility to EAC, which may be expected based on the equiaxed grain structure.

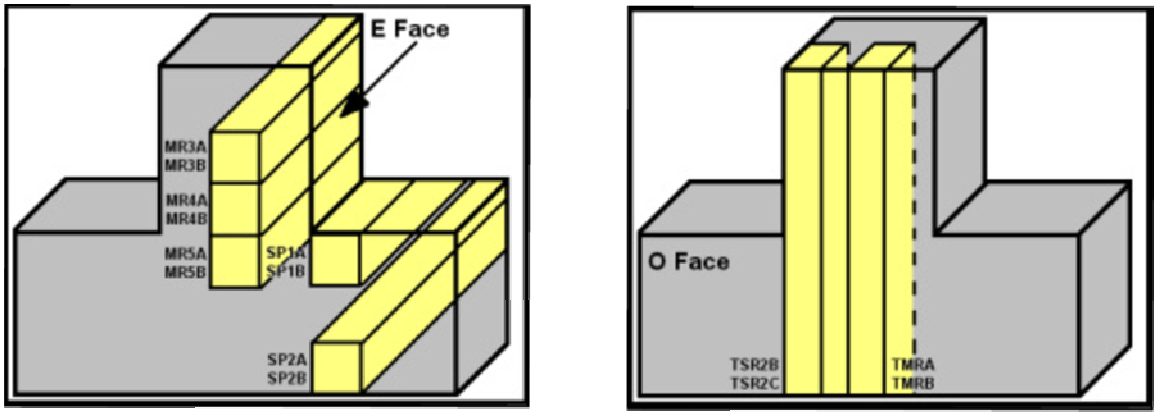

Figure 29: Locations of specimen removal for the wide panel extrusion.

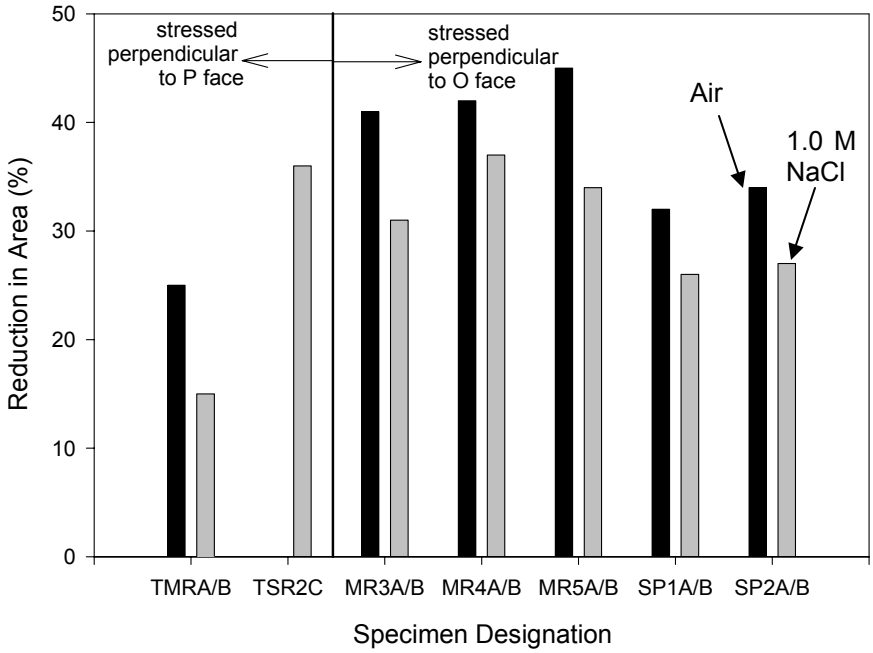

Figure 30: Reduction in area results for slow strain rate tests in the wide panel extrusion.

The variation in the RA results (Figure 30) are likely a result of the varying microstructure in the wide panel extrusion, particularly noticeable across the O plane (Figure 19). Therefore, the results for specific microstructures need to be carefully considered, rather than a simple comparison of particular orientations. In order to do this, comparisons were made using fractography and cross-sectioning, as RA measurements were not a reliable source of information due to the difficulties in pairing up microstructures. Although it was difficult to pair the structures exactly, it was possible to group the structures together by grain shape and orientation thus providing a method of comparison both to each other and to the data from the 2-inch extrusion.

Figure 31 shows the two microstructures discussed in detail below. One of the microstructures looks similar to the microstructure seen in the 2-inch extrusion from the E plane; the other microstructure is similar to the O plane in the 2-inch extrusion. However, all specimens did not have these simple microstructures. Figure 32 shows the O plane for one of the samples that were stressed perpendicular to the P plane (TSR2C). The size and shape of the grains is similar to a specimen from the O plane. However, due to the specimen removal location the grain flow direction is 45º with the specimen edge.

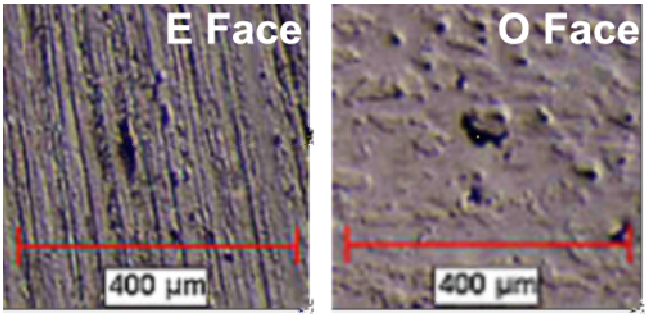

Figure 31: Microstructures of representative specimens from the wide panel extrusion (x100)

Figure 33 shows the fractographic technique previously described for measuring the ductile fracture area. Both of the samples shown in Figure 33 were stressed perpendicular to the O plane and have cross-sections similar to an E plane of the WP extrusion. The specimen in the top portion of Figure 33 was tested in air and shows 53% ductility. The bottom specimen was tested in 1.0 M NaCl and shows only 45% ductility. The areas of brittle fracture are once again much smoother and flatter in the salt-water test and the areas of ductile fracture actually show less ductility when observed at

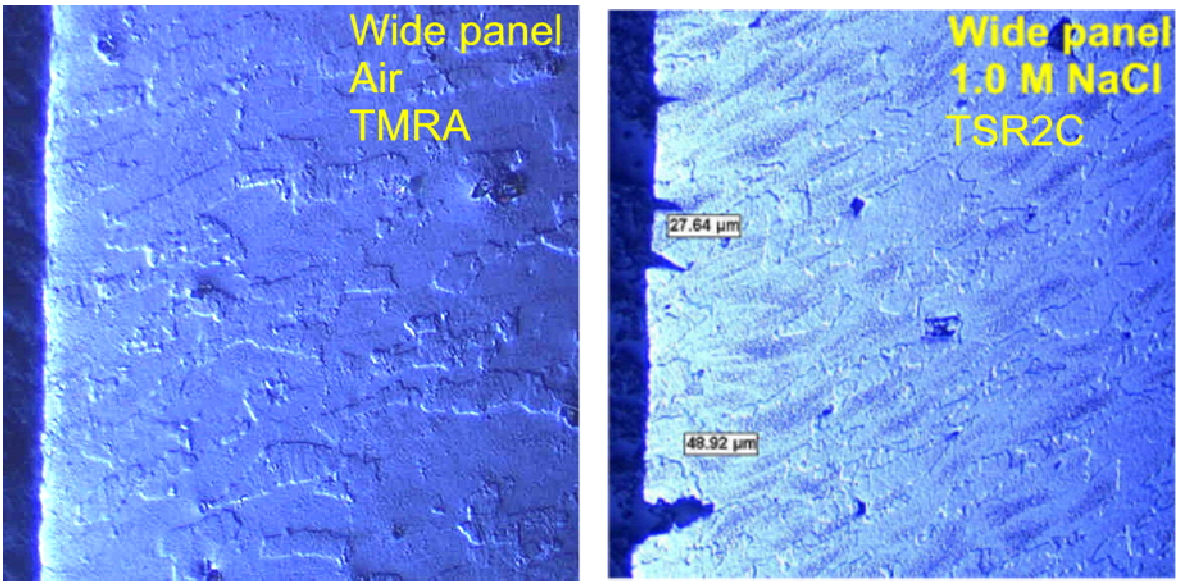

Figure 32: Cross section of sample stressed perpendicular to the P face of the WP extrusion (x200)

higher magnification.

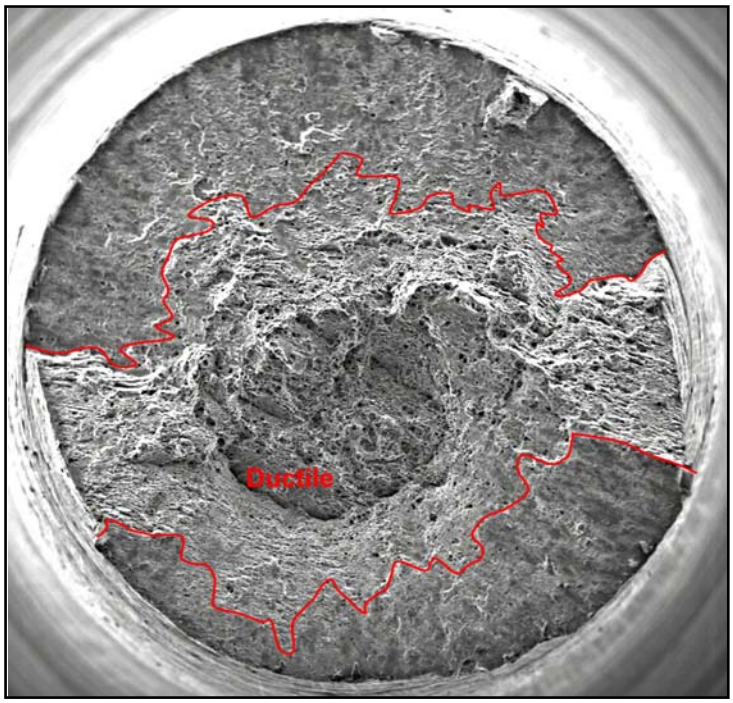

Figure 33: Fracture surfaces of WP specimens stressed perpendicular to the O face showing reduction in ductility for specimens tested in air (MR3A, above) and salt water (MR3B, below) (x77)

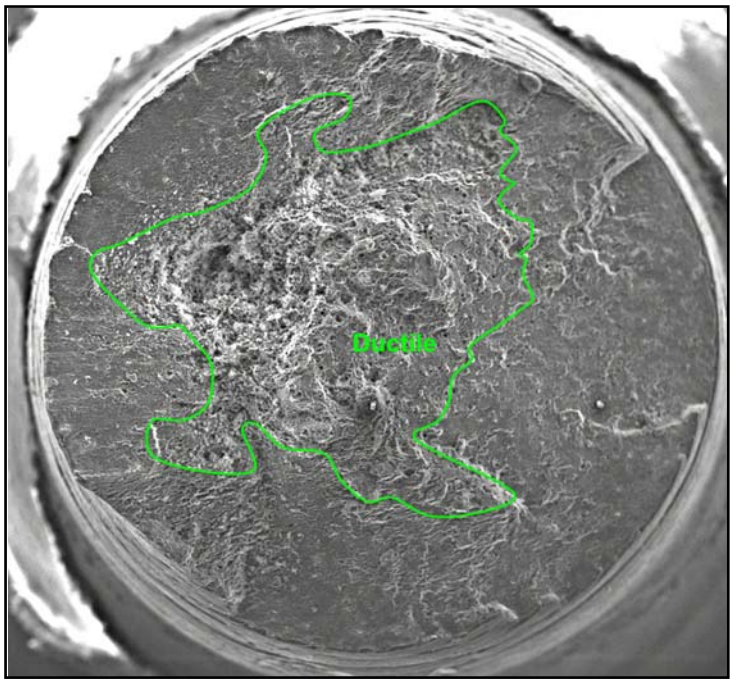

Figure 34 shows specimen cross-sections from the wide panel extrusion. Since the microstructures varied across the planes, specimens were chosen that best demonstrate a comparison to microstructures in the 2-inch extrusion. In the 1.0 M NaCl solution, the specimens once again show susceptibility to stress corrosion cracking through the formation of notches and cracks. The crack depths for the wide panel extrusion was, in general, greater than those in the 2-inch extrusion. In addition, the samples stressed perpendicular to the P plane in the wide panel extrusion, showed a much greater susceptibility than those from the 2-inch extrusion as seen in Figures 32 and 34. This data supports the trend seen in the DCB data that shows that cracks in the wide panel extrusion grow faster than cracks in the 2-inch extrusion. This trend was seen in all the samples observed. Because the duration of the test was only 24 hours, the cracks are still small; however, the presence of these cracks in all specimens, both 2-inch and wide panel, further show that AA7249 is susceptible to stress corrosion cracking, particularly when stressed perpendicular to the P plane.

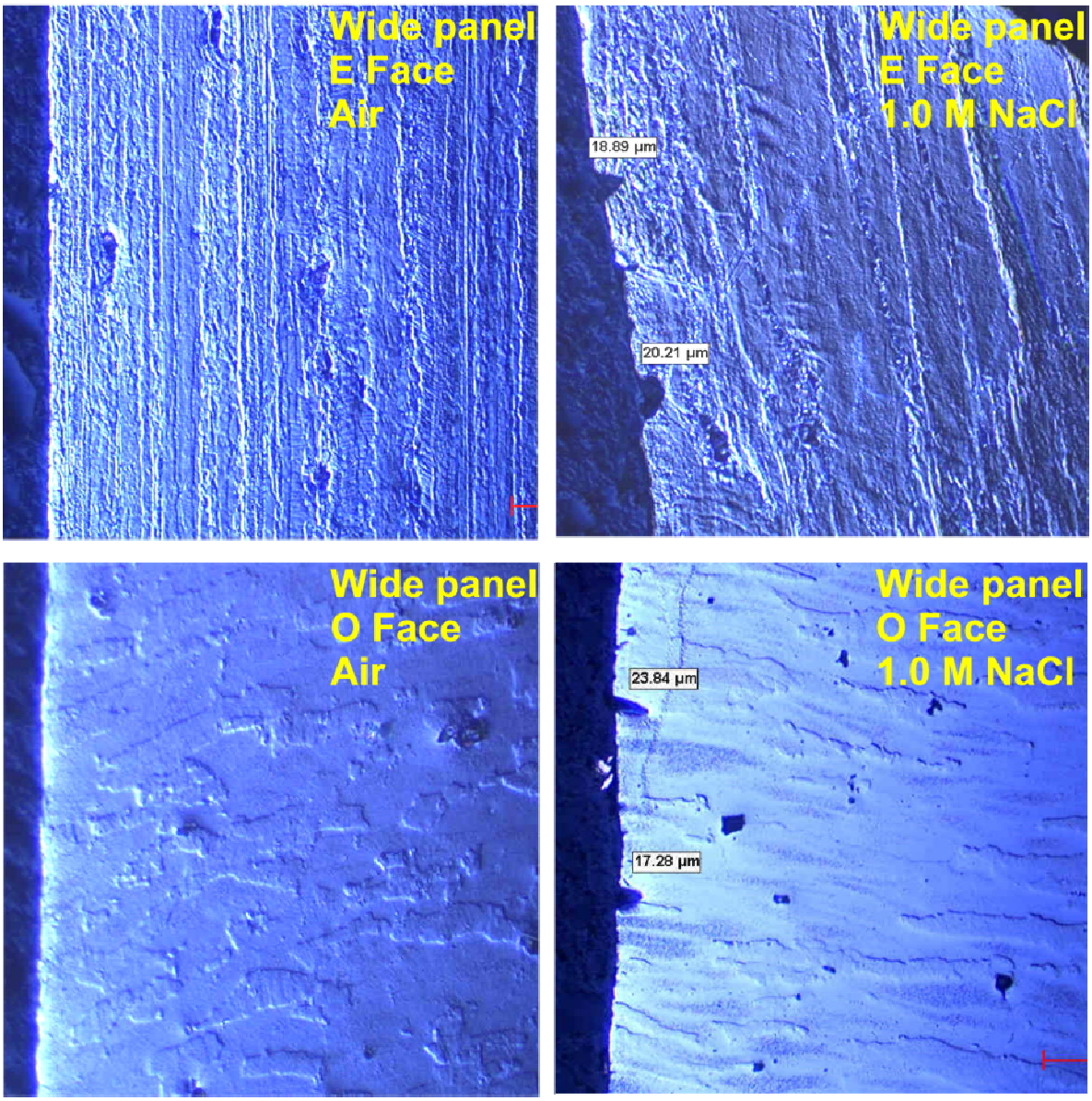

Figure 34: Cross-sections of wide panel extrusion specimen for both E face (MR3A and MR3B, top) specimen and O face-specimen (TMRA and TMRB, bottom) (x200)

Conclusions

AA7249 versus AA7075

As seen by the results of testing compared with those for AA7075, AA7249 meets or exceeds all the properties of AA7075. Not only does AA7249 outperform AA7075 mechanically, but AA7249 performs better than AA7075 in environmental testing as seen in the DCB tests as evidenced by the slower crack growth rate.

7249 SCC Susceptibility

Although AA7249 outperforms AA7075, it is not invulnerable to environmental attack. As seen in the double cantilever beam and slow strain rate testing, AA7249 is susceptible to both stress corrosion cracking initiation and propagation. These characteristics are dependent upon environment as determined by the DCB specimen in several different environments. The susceptibility of the alloy is also dependent on the microstructure. In general, when the specimens are more equiaxed, they are prone to more severe stress corrosion cracking. In addition, the wide panel extrusion is more susceptible to a faster crack growth rate once initiation has occurred.

Effects of Processing

As expected, microstructure had an effect primarily on the environmental properties of the plate. The extrusion process, which includes a heat treatment and stress relief process, typically eliminates any recrystallization that occurred during the process. This provides for extrusions that are mechanically uniform. Each specific direction (relative to the extrusion) has different microstructural characteristics; however, across each direction, the mechanical properties display little variation.

The effect of processing was particularly important in analyzing the wide panel data. Instead of relying on even the plane that the sample was from, it was important to characterize the specific grain orientation and size of each sample. The direction and orientation of the grains had an effect on the environmental response of the material. Those specimens with exposed microstructures exhibiting more equiaxed grains were more susceptible to intergranular crack propagation as compared to specimens whose grains were elongated parallel to the applied force.

Currently, caution is taken when load is applied to extrusions to ensure that the extrusion is mechanically sound. The knowledge of how microstructure affects an extrusion's susceptibility, combined with the understanding of how microstructure affects loading, will lead to the development of parts that are less susceptible to SCC, yet mechanically sound.

Recommendations

In order to compare the slow strain results effectively to other alloys, additional testing would be required, particularly on other alloys. Testing on plate AA7075 and AA7150 in both the L and ST directions would provide a basis for comparison between AA7075, AA7150, and AA7249. In addition, in order to fully characterize the effect of microstructure on SCC, it would be necessary to run tests in the other remaining directions.

In order to develop a further understanding of the extrusion process on EAC resistance, testing could be further extended to include testing extrusions produced at several different extrusion ratios.

Appendix A: DSC Data Analysis

Background on Thermal Analysis

Thermal analysis can be used for metals to determine when certain events, such as melting or phase changes, occur. This is important because the properties of a metal are very dependent upon the phases of the alloying elements. When the phases are identified, the heat treatment applied to the material can often be subsequently identified. In addition, heat treatments can be optimized once the phases are identified.

Differential Scanning Calorimetry

Figure 35: Sample and reference pan used in Differential Scanning Calorimetry (DSC)

One specific type of thermal analysis is called differential scanning calorimetry (DSC). DSC determines the temperature and heat flow associated with certain phenomena as a function of time and temperature. The DSC instrument has several parts: a chamber for the sample and reference pan, a heater and a refrigerator to provide the heat flow, and an air tank to purge inert gasses through the chamber during testing. Two pans are contained within the chamber; one pan is a reference pan that is empty; the other pan is the sample pan that contains the sample. Figure 35 shows the inside of the chamber containing both pans. The entire chamber is not heated. Instead, each platform (one for the sample, on for the reference) has its is own heater and temperature sensor. The system tries to keep the temperatures the same and measures the different amount of heat required by each platform to do so. Differential heat flow to the sample and reference pan is measured by thermocouples under the pans.

There are two different types of phenomenon that can be identified by DSC: reversible and non-reversible. Non-reversible phenomenon are such events as the curing of a two-part epoxy—once they have occurred, they cannot return to their original state. Conversely, reversible phenomenon describe events such as melting or phase changes that can return to their previous state by changing the temperature. DSC gives at least two ways to separate these phenomena. The first way to distinguish these events is by heating up the sample at different heating rates. Phenomena can be identified by a peak in the heat flow curve. When heated at different rates, these peaks occur at a constant temperature for non-reversible events and at different temperature for reversible events. Another method to distinguish these two events is by using modulated DSC. Modulation provides a constant *average* heating rate; the actual heating

rate oscillates around the average heating rate. In these tests, reversible phenomena were found by using several heating rates.

Test Procedure

Thermal analysis was conducted using a TA Instruments model 2920 DSC with 3100 Thermal Analyzer. Three samples were originally analyzed: AA7249-T6, AA7249-RRA, and AA7249-T76. The T76 condition was the alloy as received from the industry. The T6 and RRA conditions were applied to additional samples as a method of comparison between heat treatments. In addition to these samples, pieces were run from the wide panel extrusion used in testing. The heat treatment of the wide panel extrusion as received was not known; DSC was therefore run on it in an attempt to identify its heat treatment through comparison with the other samples.

Prior to beginning testing, calibration was performed using an indium standard. Three samples from each temper were run at five heating rates: 5°C/minute, 10°C/minute, 20°C/minute, 25°C/minute, and 30°C/minute. The mass of each sample was recorded to ensure that approximately 30 miligrams were tested. Although DSC samples are typically smaller, due to the magnitude of the events seen in aluminum, larger samples were necessary to identify these events.

Results

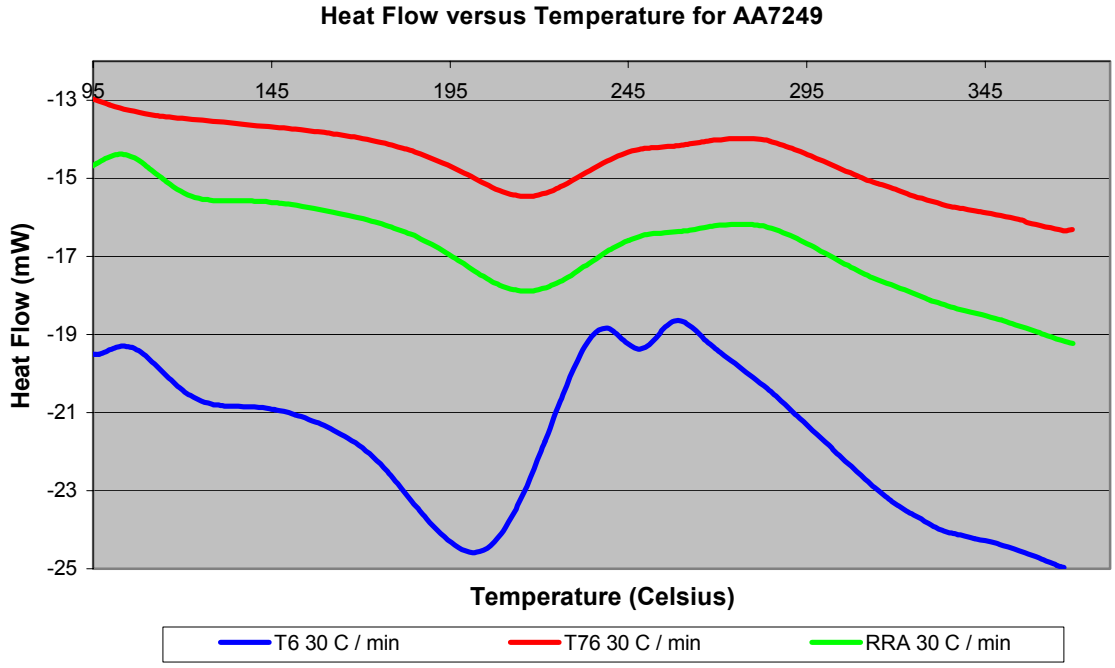

Figure 36: DSC Curves for three known heat treatments

Each of the curves in Figure 36 represents the data from a different known sample. There are a few things to notice in these curves. First, all of the peaks occur at different temperatures. This signifies that each of these events is reversible. In addition, each temper, T6, RRA, and T76 have distinct profiles.

Conclusions

The T76 and RRA curves are much closer in profile when compared to the T6 curve, particularly in regards to the second event. In the T6, this event is much more pronounced. Although it is not clear what event is occurring, this could contribute to the differences that are generally seen between T6 and T7X/RRA tempers, particularly the poor resistance of T6 to stress corrosion cracking. In order to identify what events were occurring at these temperatures, it would be necessary to conduct TEM work in conjunction with the thermal analysis.

It can also be determined that the wide panel as received was in a T7X temper. Although it was not known, wide panel extrusions are typically in T76511 tempers. This is supported by the close resemblance of the wide panel data to the T76 data.

Appendix B: Double Cantilever Beam Specimen Precracking and Loading Procedures

Precracking

Although a notch had been machined into each specimen, it was necessary to start a sharp crack tip at the end of the notch to serve as the start of the stress corrosion crack. A fatigue precrack was initiated in each specimen in accordance with ASTM standard G168-00.[47] The specimens were precracked using sinusoidal cyclic loading with a constant maximum stress intensity factor. In order to initiate a crack that was between 2.5 and 3.8 mm from the tip of the notch and to avoid exceeding the recommended stress intensity factor, a stress intensity factor of 7 was applied through the precracking. This stress intensity factor was calculated using the equation seen in Figure 37.

$$K_I = \frac{3.464 * P * a\left(1 + 0.673\left(\frac{H}{a}\right)\right)}{(B_n)^{1/2} * H^{3/2}}$$

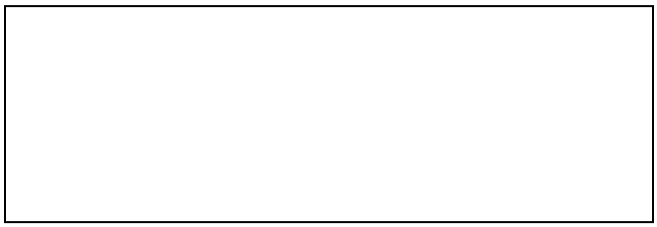

Figure 37: Equation used to calculate stress intensity factor for DCB specimen

Loading Procedures

The tests required that a constant load be placed on the bolts. This was controlled by having a constant crack mouth opening displacement (CMOD). In order to determine the CMOD, the desired load must be known. The load placed on the bolts was the load required by standard to produce 90% of the fracture toughness value at mechanical failure. This K_{IC} value was obtained from previous fracture toughness testing on the AA7249 and by loading a DCB specimen until fracture. At fracture an audible "pop" was heard and the crack mouth opening displacement was measured. This point provided an estimate of K_{IC} that was converted into the critical stress intensity value. A CMOD was calculated using the equation for crack mouth opening displacement provided in ASTM standard G168-00. The equation shown in Figure 38 was used to calculate this value at 90% of K_{IC}.

$$V_o = 2.309\left(\frac{K_{IC}}{E}\right)H^{1/2}\left(\frac{a_o}{H}+0.673\right)^2\left[1+1.5\left(\frac{c_o}{a_o}\right)-1.15\left(\frac{c_o}{a_o}\right)^2\right]$$

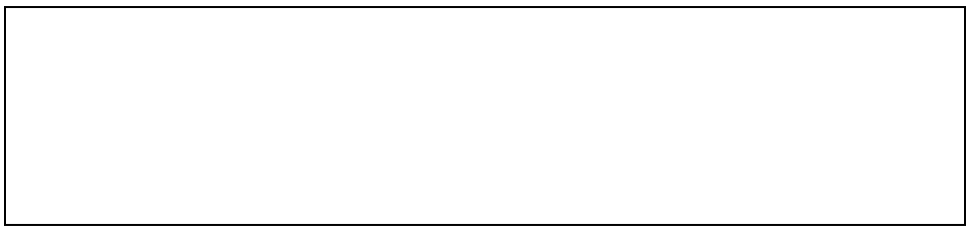

Figure 38: Equation used to calculate initial crack mouth opening displacement for DCB specimen

Once each specimen was fatigue precracked, the specimens were bolt-loaded. A bolt was inserted to each hole on the top of the specimen. The bolts were then moved close to each other, but not yet in contact. At this time, the clip gage was put in the crack mouth opening. The clip gage was then zeroed and the bolts were tightened until contact was made. Once touching, an even torque was applied to the bolts simultaneously by hand. Once the clip gage read the predetermined final crack mouth opening displacement, it was removed. The specimens were then dipped into an epoxy to prevent the formation of a galvanic cell between the bolts and the specimen once it was placed in an environment. Immediately after being dipped in epoxy, the specimens were placed into their environment and measured for the first time. These measurements were continued until the crack stopped growing, which occurred when the stress intensity factor reached the stress intensity factor for stress corrosion cracking, K_{ISCC}. After the cracks stopped growing, the specimens were fractured and examined via scanning electron microscopy. Prior to fracture, the specimen was subjected to cyclic loading in order to mark the end of the stress corrosion crack.

Appendix C: Phase I Raw Data

Hardness Measurements

On each hardness specimen, a 1/8-inch by 1/8-inch grid outlined the measurement locations. Measurements were taken at the middle of each square and recorded. Statistical analysis was done on the measurements in the same groups as the conductivity measurements as a means to provide comparison. Hardness measurements were then plotted in a contour plot to determine the presence of trends. Four risers and the two-inch specimen were measured in this manner. The results from riser two are represented below.

Riser #2

	Left					Center								Right					
Top Riser										88.4	88.6	88.7	88.5						
										89.3	89.7	89.9	89.4						
										89.6	89.9	90.0	90.0						
Bottom Riser										90.2	90.3	90.3	91.1						
										90.1	89.9	90.1	90.2						
										90.1	89.9	89.6	90.0						
										89.4	89.5	90.0	89.9						
Top Plate	89.4	89.9	89.1	88.8	88.5	88.2	88.7	89.9	89.9	89.5	89.8	89.8	90.0	89.9	89.8	88.7	87.9	88.3	88.3
	89.6	90.2	90.5	90.4	90.2	90.2	90.4	90.0	89.9	89.9	90.0	90.1	90.2	90.1	90.1	90.1	90.2	90.1	90.2
	89.9	89.7	89.9	89.9	90.0	90.0	90.0	89.8	89.7	89.9	89.8	89.7	89.7	89.9	89.9	90.2	90.0	90.0	90.0
Bottom Plate	89.1	89.9	90.4	90.7	89.8	89.8	89.9	90.0	90.1	90.1	89.9	90.1	90.2	90.1	90.1	89.9	90.2	89.9	89.9
	89.0	89.2	88.5	89.1	88.8	90.4	89.2	89.4	89.7	89.2	89.5	89.6	89.7	90.7	90.0	89.8	90.1	90.8	89.7

Statistics	Location						
	Riser	Plate	Top Plate	Bottom Plate	Under Riser	Not Under Riser	Whole
Mean	89.7	89.8	89.7	89.8	89.8	89.7	89.8
Number of Data Points	28	95	57	38	20	75	123
Standard Deviation	0.606	0.563	0.592	0.521	0.260	0.619	0.571
Min	88.4	87.9	87.9	88.5	89.2	87.9	87.9
Max	91.1	90.8	90.5	90.8	90.2	90.8	91.1

Figure 39: Raw data for hardness measurements and statistical analysis on the measurements (HRB)

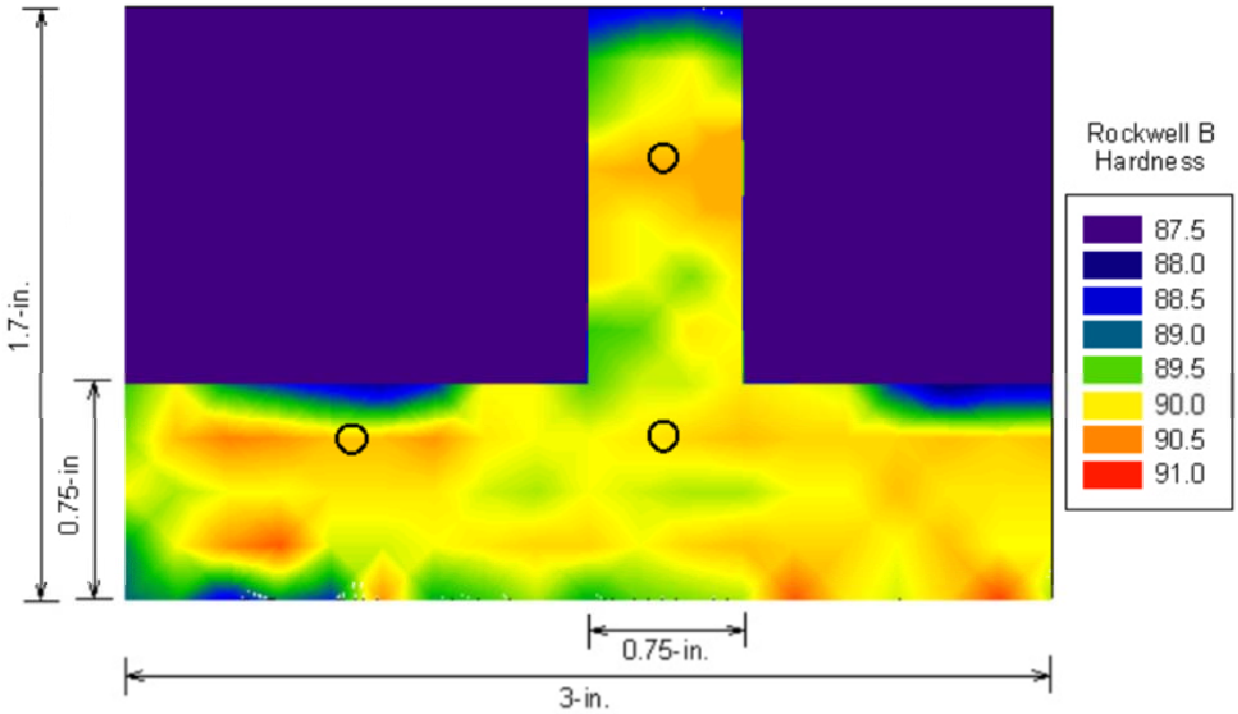

Figure 40: Contour map for hardness measurements on Riser #2

Tensile Testing

Tensile specimens were taken from both the wide panel and two-inch extrusion. Specimens were taken after completion of initial microscopy, hardness measurements, and conductivity measurements. Because the hardness and conductivity measurements did not show any significant variation, selection of locations for tensile specimens was based primarily upon the microstructure. All specimens were taken in the direction of extrusion (L) as tensile specimens are typically taken in this direction for evaluation and comparison of properties. Three tensile specimens were removed from each location.

Analysis of the data was done using the position and load values returned from the test machine. Engineering stress (σ) and strain (ε) were calculated using the equations shown in Figure 41.

$$\sigma = \frac{F}{A} \qquad \varepsilon = \frac{l - l_i}{l_i}$$

σ	=	Engineering stress, lb/in^2
F	=	Force (load), lb
A	=	Original cross-sectional area, in^2
ε	=	Strain, in/in
l_i	=	Original gage length, in
l	=	Gage length, in

Figure 41: Equations for engineering stress and strain

The results of these tests were then plotted and analyzed according to ASTM standard B557-94. A linear regression was performed for the straight-line portion of the data, standardized across all tests by taking the data between 30,000 lb/in^2 and 60,000 lb/in^2. The slope of this line, also known as Young's Modulus of Elasticity, was then shifted over 0.0002 in/in on the x-axis to begin the 0.2% offset line. This line was extended to find the intersection between the 0.2% offset line and the raw data. The intersection of these curves is the yield strength that defines the first failure, the onset of plastic deformation. Ultimate yield strength was determined by finding the maximum load on the specimen and dividing by original cross-sectional area. Figure 42 shows a plot for one of the tensile specimen with the 0.2% offset line plotted.

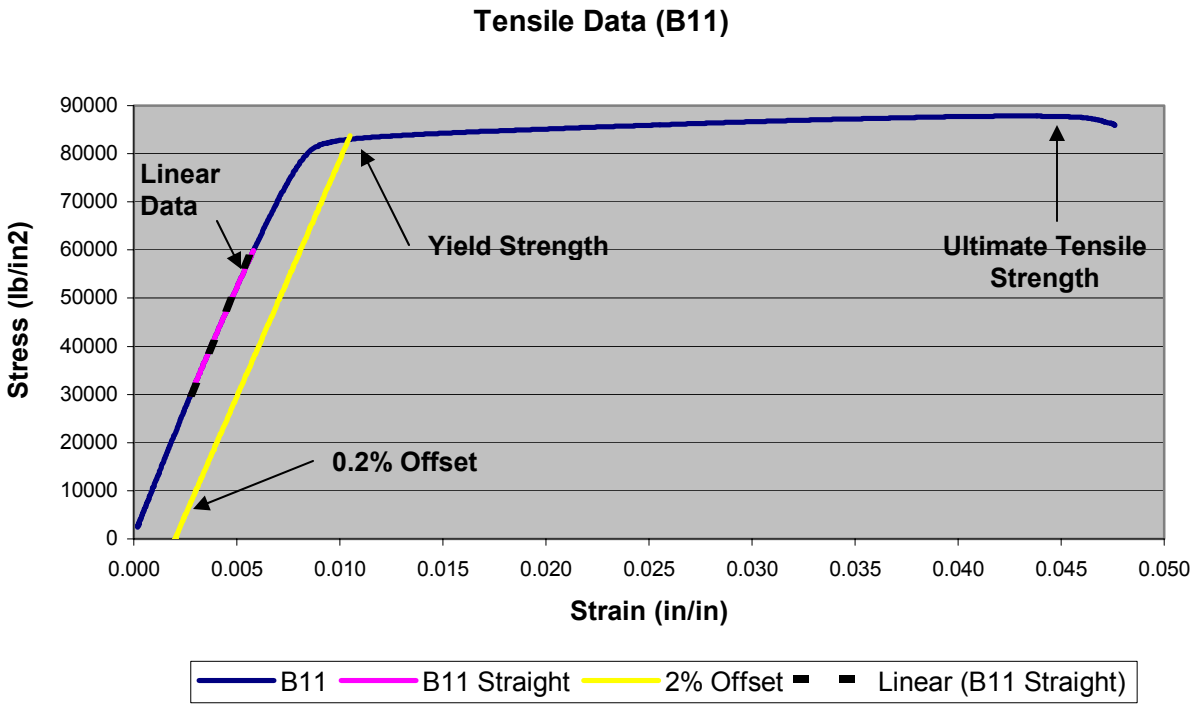

Figure 42: Sample tensile data

Statistical analysis was performed on the resulting data in each location. The results are shown in Table 6. Tests that resulted in extensometer slippage were discarded. Evidence of extensometer slippage is seen in the plot; Figure 43 is an example of a plot with extensometer slippage.

Table 6: Raw data and statistical analysis for tensile tests

Sample	Test Number	Original Diameter	Original Area	Yield Strength	Tensile Strength	Young's Modulus
		in	in^2	ksi	ksi	10^6 ksi
4B	042	0.126	0.0125	79.15	85.28	9.75
4C	041	0.126	0.0125	80.10	85.31	9.78
4D	040	0.126	0.0125	78.98	85.36	9.34
4E	038	0.126	0.0125	77.68	82.32	9.60
4F	039	0.126	0.0125	78.24	83.03	9.25
7A	032	0.126	0.0125	81.72	86.11	9.68
7C	034	0.127	0.0127	79.24	84.95	9.52
7D	035	0.127	0.0127	79.40	84.43	9.80
7F	037	0.127	0.0127	78.81	82.80	9.90
B11	024	0.127	0.0127	83.68	87.84	9.84
B13	026	0.127	0.0127	81.95	86.81	9.70

Table 6 (continued): Raw data and statistical analysis for tensile tests

		Wide Panel Extrusion				2-inch Extrusion	
		Top Riser	Under Riser	Not Under Riser	Whole	Middle	Whole
YTS	Mean	80.44	79.43	78.24	79.26	81.95	82.82
	Number of Points	2	4	3	9	1	2
	Standard Deviation	1.82	0.48	0.57	1.15	---	1.22
	Min	79.15	78.98	77.68	77.68	81.95	81.95
	Max	81.72	80.10	78.81	81.72	81.95	83.68
UTS	Mean	85.70	85.01	82.72	84.40	86.81	87.33
	Number of Points	2	4	3	9	1	2
	Standard Deviation	0.59	0.43	0.36	1.35	---	0.73
	Min	85.28	84.43	82.32	82.32	86.81	86.81
	Max	86.11	85.36	83.03	86.11	86.81	87.84
Modulus	Mean	9.72	9.61	9.58	9.62	9.70	9.77
	Number of Points	2	4	3	9	1	2
	Standard Deviation	0.05	0.22	0.33	0.22	---	0.10
	Min	9.68	9.34	9.25	9.25	9.70	9.70
	Max	9.75	9.80	9.90	9.90	9.70	9.84

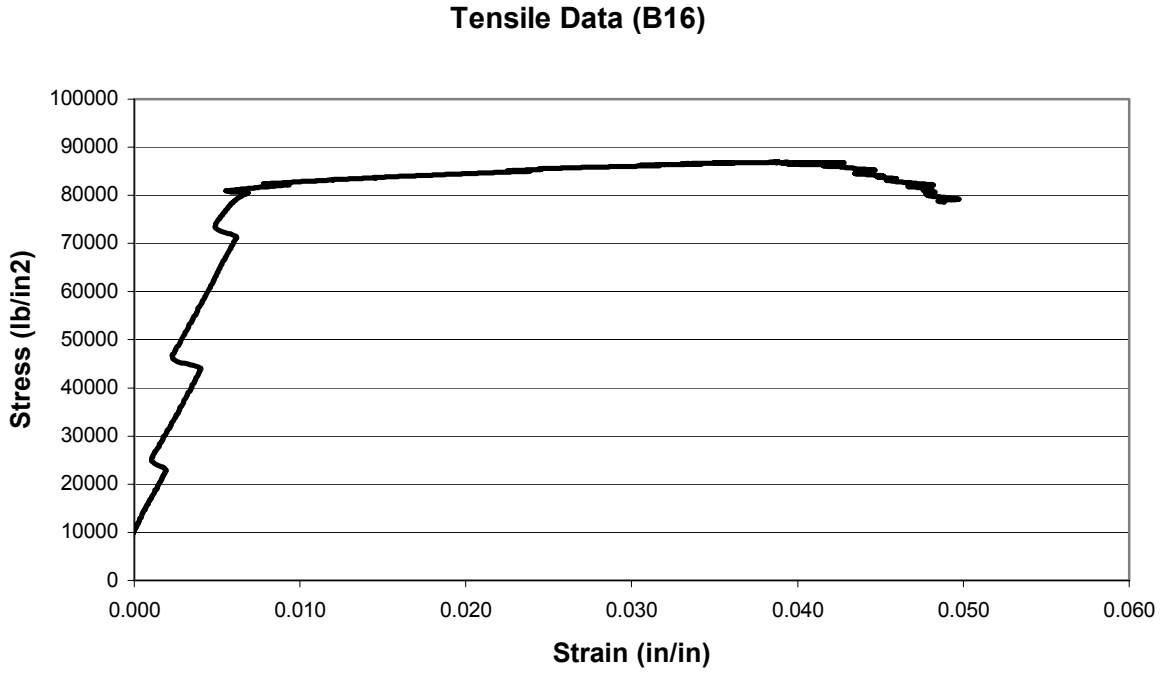

Figure 43: Tensile data showing extensometer slippage

Conductivity Measurements

Conductivity measurements were taken in several locations throughout the specimen. The proximity of the measurements was based upon the resolution of the eddy current probe. Each measurement was repeated three times and recorded. An average reading was used for each location. Statistical analysis was performed for several combinations of locations to determine if there was any variation across the sample. The cross section of three risers and the two-inch extrusion were measured. Represented below are the measurements for one of the risers and the statistical analysis performed on it.

Table 7: Raw data and statistical analysis for conductivity measurements (%IACS)

		Riser #2			
		Left		Center	Right
		A	B	C	D
Top Riser	1			38.6	
				38.6	
				38.5	
Bottom Riser	2			38.5	
				38.5	
				38.5	
Top Plate	3	38.1	38.3	38.5	38.3
		38.1	38.2	38.5	38.1
		38.1	38.2	38.5	38.1
Bottom Plate	4	38.4	38.4	38.3	38.3
		38.3	38.4	38.4	38.1
		38.3	38.4	38.3	38.1

Statistics	Location						
	Riser	Plate	Top Plate	Bottom Plate	Under Riser	Not Under Riser	Whole
Mean	38.5	38.3	38.3	38.3	38.4	38.2	38.3
Number of Data Points	6	24	12	12	6	18	30
Standard Deviation	0.052	0.141	0.168	0.108	0.098	0.124	0.164
Min	38.5	38.1	38.1	38.1	38.3	38.1	38.1
Max	38.6	38.5	38.5	38.4	38.5	38.4	38.6

Appendix D: Phase II Raw Data: DCB Data Analysis

Test Matrix

The DCB specimens were set up to provide two different comparisons. The first comparison was to compare the susceptibility of the 2-inch extrusion with that of the wide panel extrusion. In addition, specimens drawn from the 2-inch extrusion were placed in several different environments to determine the susceptibility of AA7249 in different environments. The test matrix is shown in Table 8.

Table 8: Specimen used in DCB Measurements

Environment	Extrusion	Specimen Numbers		
0.6 M NaCl Dropwise	Wide panel	7249-WP-2	7249-WP-4	7249-WP-6
		7249-B2-01	7249-B2-02	7249-B2-10
0.6 M NaCl Dropwise	2-inch	7249-B2-12	7249-B3-22	7249-B3-24
0.05 M NaCl	2-inch	7249-B2-05	7249-B2-14	7249-B3-25-2
0.10 M NaCl	2-inch	7249-B2-06	7249-B2-15	7249-B3-27
0.60 M NaCl	2-inch	7249-B2-07	7249-B2-08	7249-B3-29
		7249-B2-03	7249-B2-09	7249-B2-13
1.00 M NaCl	2-inch	7249-B2-17	7249-B3-30	---

Crack growth vs. Time

Crack growth versus time plots were generated directly from the raw data. The time was measured from the time the specimens were first placed into their environment. Measurements were made on a daily basis until the crack growth slowed. Each curve contains the crack growth for each specimen in the same environment. Plots used for analysis were the plots generated for the dropwise specimen. In these plots, the data was generally split up into two sections: constant crack growth rate and crack growth arrest. After loading, the specimen showed constant crack growth, representing Stage II crack propagation—constant crack growth velocity. At the end of Stage II propagation, the crack growth slowed and eventually stopped once the critical stress intensity was reached. This is shown in the second section of the data by the leveling out of the readings around the final crack length. In the first three specimens, the data had a third section to it that occurred before the other two stages. After initial loading, there was often a short period of non-linear crack growth. This data is expected to come from the end of Stage III crack propagation. The value used for comparison between the 2-inch and wide panel extrusion was the slope of the linear data—the value of constant crack rate propagation. Each of the graphs below shows the raw data for each of the dropwise specimens. On the graph is also a horizontal line that represents the final crack length, a straight line that was fit through the linear data, and the equation of the fit line.

Figure 44: Double Cantilever Beam Specimen: 2-inch Extrusion

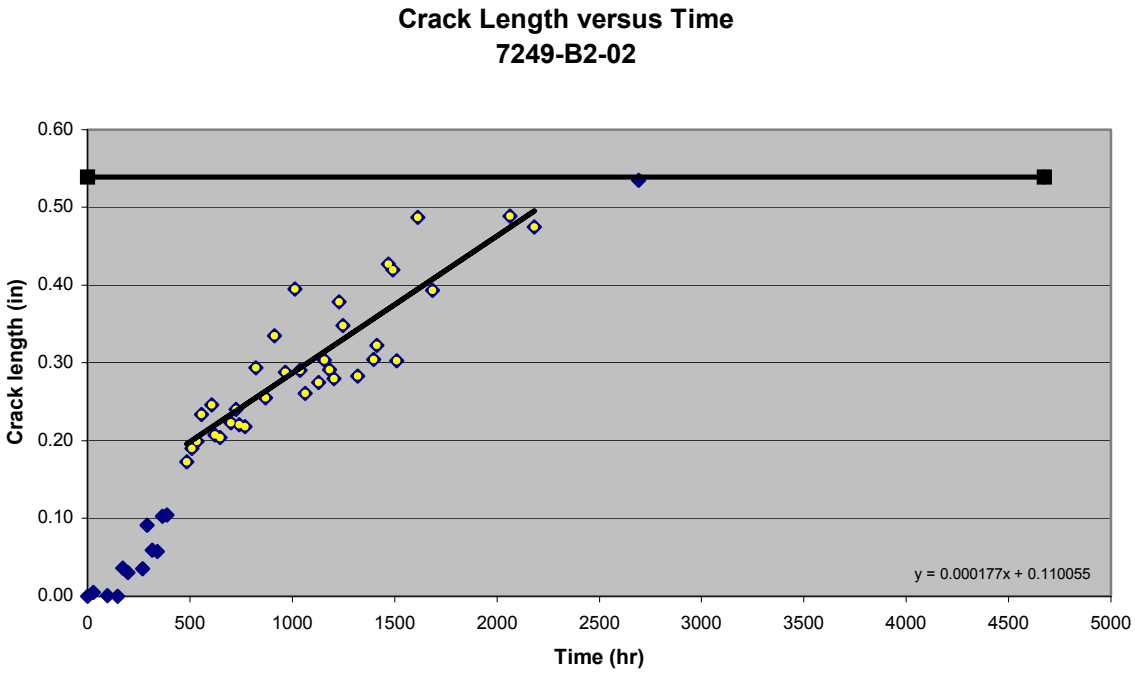

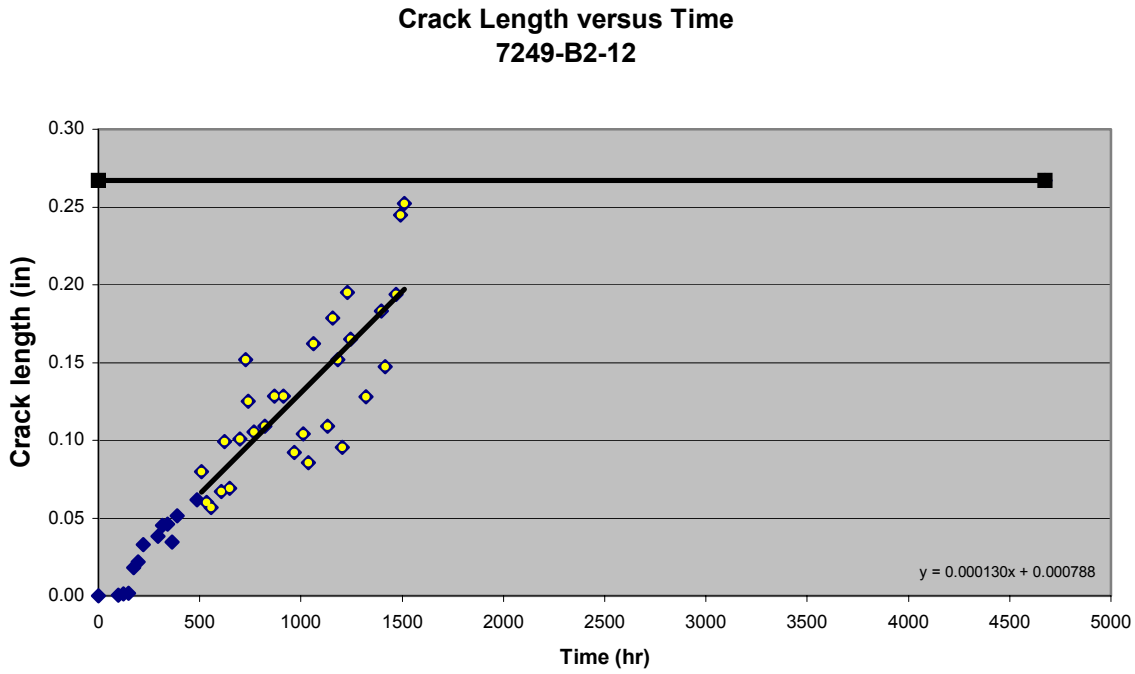

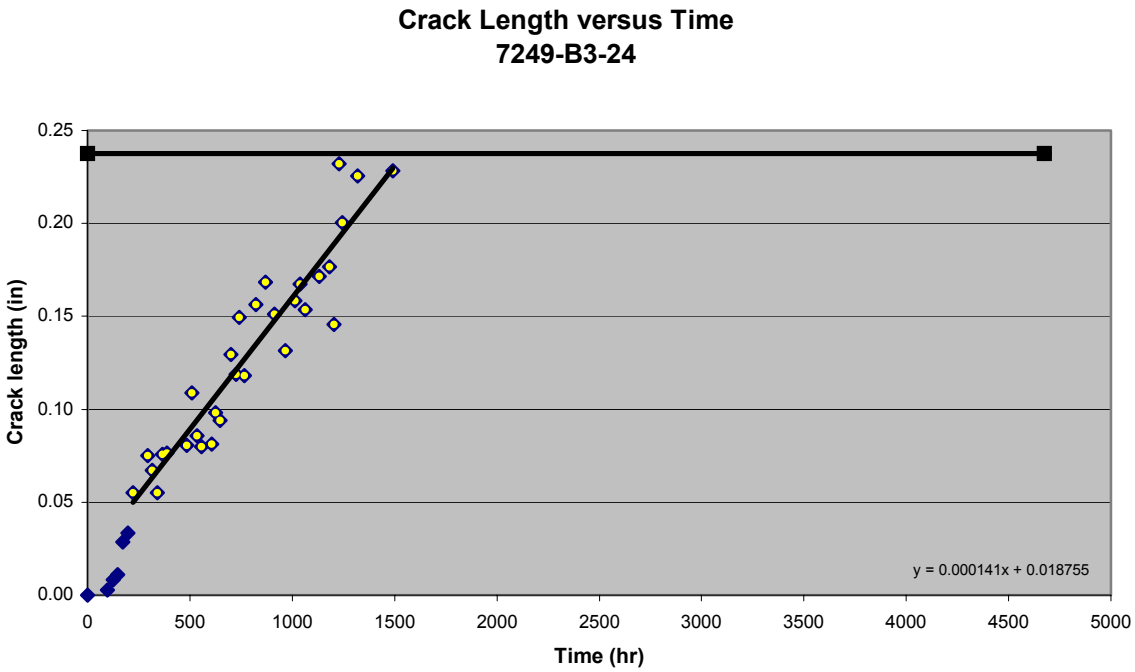
Crack Length versus Time
7249-B3-24
Crack length (in)
0.25
0.20
0.15
0.10
0.05
0.00
0
500
1000
1500
2000
2500
3000
3500
4000
4500
5000
Time (hr)
y = 0.000141x + 0.018755

Figure 45: Double Cantilever Beam Specimen: Wide Panel Extrusion

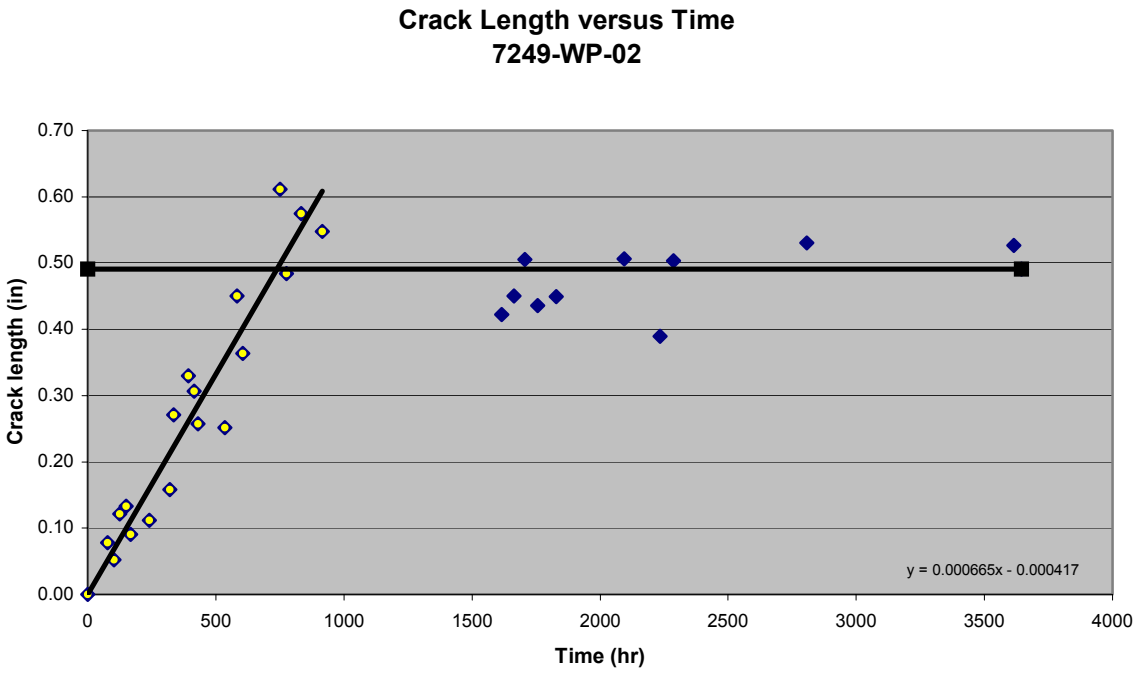

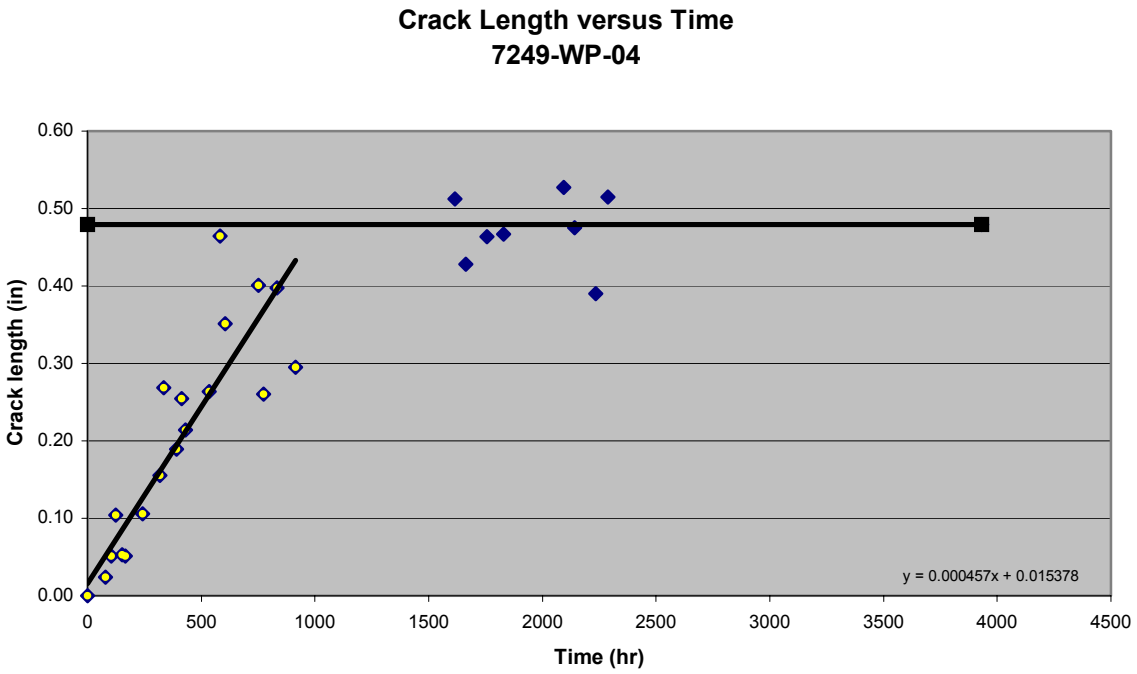

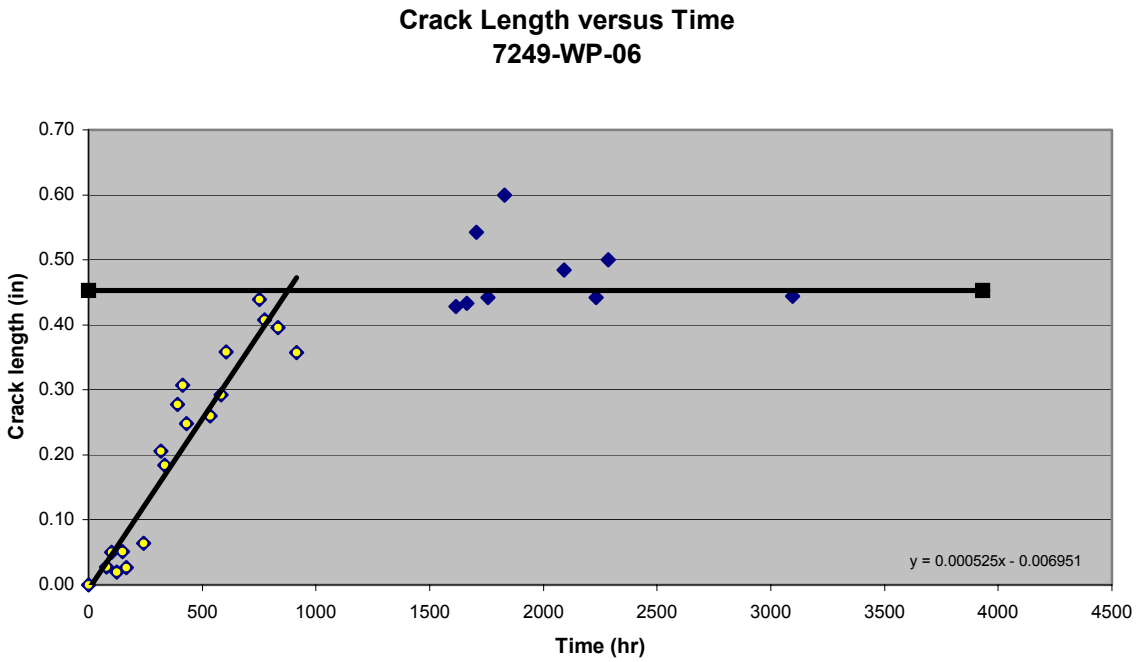
Crack Length versus Time
7249-WP-06
Crack length (in)
0.70
0.60
0.50
0.40
0.30
0.20
0.10
0.00
0
500
1000
1500
2000
2500
3000
3500
4000
4500
Time (hr)
y = 0.000525x - 0.006951

The remainder of the data is the raw data for the remaining specimen. The data was plotted simultaneously as a method to compare the effect of the environment on crack growth. From the data shown in Figure 46, it is clear that AA7249 is susceptible to stress corrosion cracking in even dilute environments. The data also shows two different sections to the crack growth as seen in the dropwise specimen. At first, there is non-linear crack growth. This crack growth is similar for all of the specimens. However, as the cracks begin to reach steady-state crack growth propagation, the slopes of the lines begin to change. For example, although the 1.0 M NaCl specimens take a longer time to grow steadily, once begun, the crack growth rate is faster than any of the other specimens as evidenced by the steeper slope of the line.

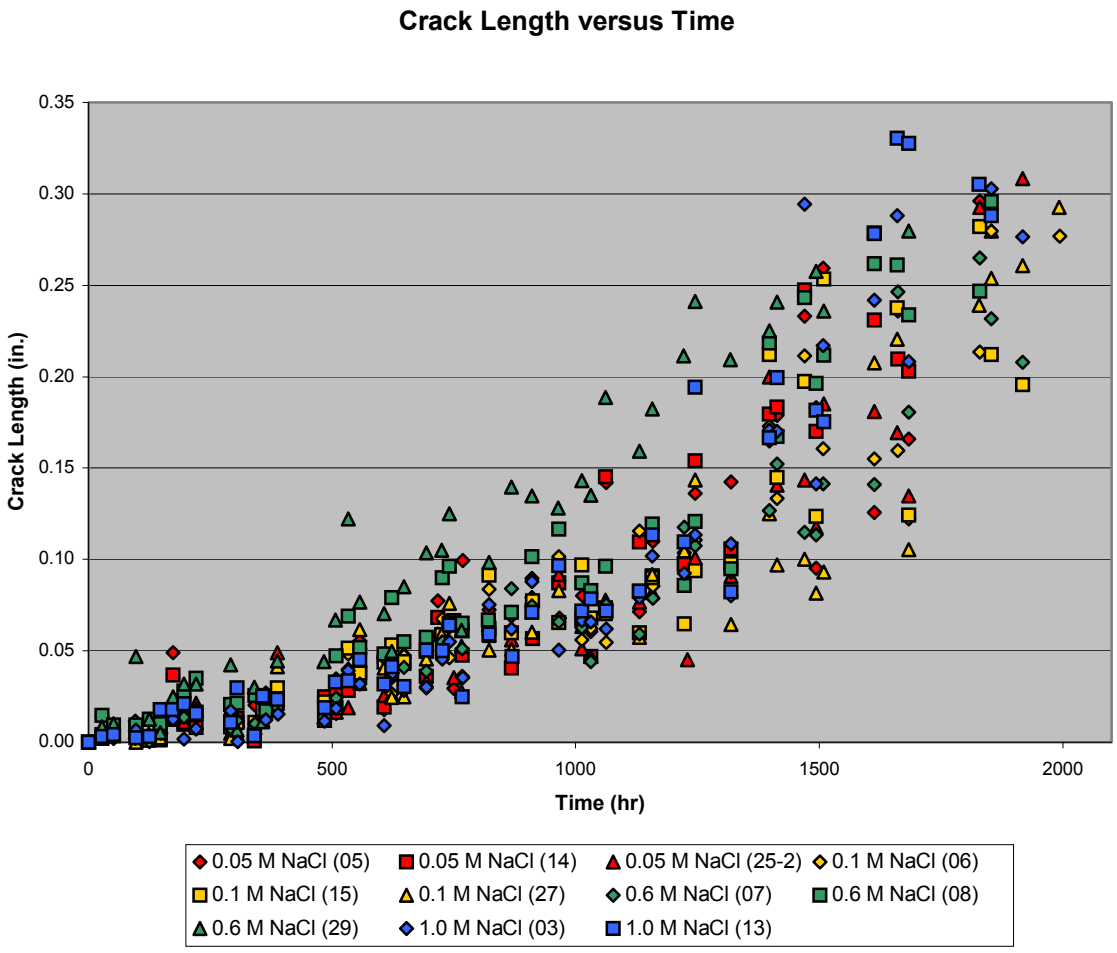

Figure 46: Crack growth rate versus time for 2-inch specimen immersed in several different solutions

The environment thus plays a role in the crack rate propagation in a material. Future work could include a comparison between specimens from different extrusions such as AA7075 and AA7150 compared to that of AA7249.

Appendix E: Phase II Raw Data: Slow Strain Rate Technique

Sample Preparation and Testing

Each sample was a sub-sized tensile specimen machined according to ASTM standard G129-95. Prior to testing, the samples were hand ground with 600-grit emery polishing paper. Samples were then cleaned with acetone followed by ethyl alcohol.

Samples to be tested in salt water were placed in the grips and then painted with Intrelux epoxy to prevent any reaction between the specimen and the grips. The cell was placed around the specimen upon drying. The entire gage section of the specimen was immersed in the solution for the duration of the test.

Specimens in both environments, air and 1.0 M NaCl, were preloaded in the test rig to 300 pounds. The extension rate, based on results found in the literature, used for both the preloading and the test was 1.0×10^{-6} in/s. While to bottom of the rig was rigidly attached, the top of the rig extended slowly with the specimen attached. The position of the rig was measured and recorded. The test ran until failure, on average approximately 20 hours. At failure, specimens were cleaned and preserved for fractography and cross-sectioning.

Testing Evaluation

A specific standardized method of evaluating slow strain rate testing has yet to be developed. Slow strain rate testing, rather than providing information directly applicable, is rather a comparison of susceptibility to stress corrosion cracking between a control and test environment. There are several methods of comparing the reaction of the material in both environments. Some of these include: changes in time-to-failure, specimen elongation, reduction in area, or visual indication of stress corrosion cracking. Often a combination of these methods is used to indicate a material's susceptibility to stress corrosion cracking.

Several methods were attempted to quantify the results of the test. Initially, tensile strength, Young's Modulus, and elongation were plotted from the raw data. These plots showed slight variation in the elongation, however, trends were not clear. Reduction in area was then calculated for each specimen. The reduction in area measurements have been combined with both fractography and optical microscopy to best describe the susceptibility seen in AA7249.

References

[1] Jacobson, G.A., "Corrosion Costs and Preventative Strategies in the United States." *Supplement to Materials Performance.* (2002).

[2] Jacobson, G.A., "Corrosion Costs and Preventative Strategies in the United States." *Supplement to Materials Performance.* (2002).

[3] Hoffman, M.E., and Hoffman, P.C., International Journal of Fatigue, Vol 23: p. S1, 2001.

[4] Bucci, R.J., Warren, C.J., and Starke, E.A., Journal of Aircraft, Vol 37, No. 1: p. 122, 2000.

[5] "P-3 Orion." Military Analysis Network. Dec. 27, 1999. 12 Jan. 2002. Netscape 6. <http://www.fas.org/man/dod-101/sys/ac/p-3.htm>

[6] "Statement of Work, P-3C Service Life Assessment Program, Phases II and III." (1998): 13. 12 Jan. 2002. <http://www.fas.org/man/dod-101/sys/ac/docs/Sowa03.pdf>

[7] "Statement of Work, P-3C Service Life Assessment Program, Phases II and III." (1998): 4. 12 Jan. 2002. <http://www.fas.org/man/dod-101/sys/ac/docs/Sowa03.pdf>

[8] D. Tenney, S.S. Brown, J.R. Whitehead, T.H. Williams, "7249-T76511 Materials Qualification for the P-3 Service Life Extension Program." 12th AeroMat Conference (2001).

[9] Ferrer, C.P., "Optimizing the Strength and SCC resistance of Aluminum Alloys used for Refurbishing Aircraft," Trident Scholar project report, no. 281, United States Naval Academy, Annapolis, MD, 2001.

[10] J.R. Davis and Associates, "General Introduction." *ASM Specialty Handbook: Aluminum and Aluminum Alloys.* Materials Park, OH: 1993.

[11] J.R. Davis and Associates, "General Introduction." *ASM Specialty Handbook: Aluminum and Aluminum Alloys.* Materials Park, OH: 1993.

[12] W.H. Hunt and J. T. Staley, "High Strength Aluminum Alloys for Aerospace Application." *Light-Weight Alloys for Aerospace Applications* (1989), 111-120.

[13] D. A. Lukasak and R. M. Hart, "Aluminum Alloy Development." *Aerospace Engineering* (Sept 1991), pp 21-24.

[14] J. J. Thompson, E. S. Tankins, V. S. and Agarwala, "A Heat Treatment for Reducing Corrosion and Stress Corrosion Cracking Susceptibilities in 7XXX Aluminum Alloys." *Materials Performance* (1987) pp 45-52.

[15] J. J. Thompson, E. S. Tankins, V. S. and Agarwala, "A Heat Treatment for Reducing Corrosion and Stress Corrosion Cracking Susceptibilities in 7XXX Aluminum Alloys." *Materials Performance* (1987) pp 45-52.

[16] E. DiRusso, M. Conserva, F. Gatto, and H. Markus, "Thermomechanical Treatments on High Strength Al-Zn-Mg- (Cu) Alloys." *Metallurgical Transactions*, Volume 4 (1973), pp 1133-1144.

[17] W.H. Hunt and J. T. Staley, "High Strength Aluminum Alloys for Aerospace Application." *Light-Weight Alloys for Aerospace Applications* (1989), pp 111-120.

[18]B. M. Cina, "Reducing the Susceptibility of Alloys, Particularly Aluminum Alloys, to Stress Corrosion Cracking," U.S. Patent 3,856,584, December 24, 1974.

[19] J. K. Park and A. J. Ardell, "Effect of Retrogression and Reaging Treatments on the Microstructure of Al-7075-T651." *Metallurgical Transactions A*, Volume 15A (1984), pp 1531-1543.

[20] Ferrer, C.P., "Optimizing the Strength and SCC resistance of Aluminum Alloys used for Refurbishing Aircraft," Trident Scholar project report, no. 281, United States Naval Academy, Annapolis, MD, 2001.

[21] J.E. Hatch, *Aluminum: Properties and Physical Metallurgy*. American Society for Metals (1984) pp 47-53.

[22] D. Tenney, S.S. Brown, J.R. Whitehead, T.H. Williams, "7249-T76511 Materials Qualification for the P-3 Service Life Extension Program." 12th AeroMat Conference (2001).

[23] P.K. Saha. *Aluminum Extrusion Technology*. Materials Park, OH: 2000.

[24]D.O. Sprowls and R.H. Brown, Metals Progress 81, 5 (1962), p. 77.

[25] P.K. Saha. *Aluminum Extrusion Technology*. Materials Park, OH: 2000.

[26] P.K. Saha. *Aluminum Extrusion Technology*. Materials Park, OH: 2000.

[27] Speidel, M.O. and Hyatt, M.V., "Stress-Corrosion Cracking of High Strength Aluminum Alloys." *Advances in Corrosion Science and Technology*. Vol 2, p115-335. New York, NY. 1972

[28] Bucci, R.J., Warren, C.J., and Starke, E.A., Journal of Aircraft, Vol 37, No. 1: p. 122, 2000.

[29] J.R. Davis and Associates, "Corrosion Behavior." *ASM Specialty Handbook: Aluminum and Aluminum Alloys*. Materials Park, OH: 1993.

[30] J.R. Davis and Associates, "Corrosion Behavior." *ASM Specialty Handbook: Aluminum and Aluminum Alloys*. Materials Park, OH: 1993.

[31] R.H. Jones and R.E. Ricker. "Mechanisms of Stress Corrosion Cracking." *Stress Corrosion Cracking: Materials Performance and Evaluation*. Materials Park, OH: 1992.

[32] J.R. Davis and Associates, "Corrosion Behavior." *ASM Specialty Handbook: Aluminum and Aluminum Alloys*. Materials Park, OH: 1993.

[33] R.H. Jones. "Stress Corrosion Cracking of Aluminum Alloys." *Stress Corrosion Cracking: Materials Performance and Evaluation*. Materials Park, OH: 1992.

[34]R.H. Brown, D.O. Sprowls and M.B. Shumaker, "The Resistance of Wrought High Strength Aluminum Alloys to Stress Corrosion Cracking," in Stress Corrosion Cracking of Metals – A State of the Art, ASTM STP 518, (Philadelphia, PA: American Society for Testing and Materials, 1972), p. 87.

[35] "Standard Test Methods of Tension Testing Wrought and Cast Aluminum- and Magnesium-Alloy Products." *Annual Book of ASTM Standards*, Vol 02.02. West Conshohocken, PA: 2001.

[36] D.R. Askeland. *The Science and Engineering of Materials*. Second Edition. Boston, MA: 1989.

[37] D.R. Askeland. *The Science and Engineering of Materials*. Second Edition. Boston, MA: 1989.

[38] "Standard Practice for Determining Electrical Conductivity Using the Electromagnetic (Eddy-Current) Method." *Annual Book of ASTM Standards,* Vol 03.03. West Conshohocken, PA: 1999.

[39] "Standard Practice for Making and Using Precracked Double beam Stress Corrosion Specimens." *Annual Book of ASTM Standards*, Vol 03.02. West Conshohocken, PA: 2001.

[40] "Standard Practice for Slow Strain Rate Testing to Evaluate the Susceptibility of Metallic Materials to Environmentally Assisted Cracking." *Annual Book of ASTM Standards*, Vol 02.02. West Conshohocken, PA: 1998.

[41] "Standard Practice for Slow Strain Rate Testing to Evaluate the Susceptibility of Metallic Materials to Environmentally Assisted Cracking." *Annual Book of ASTM Standards*, Vol 02.02. West Conshohocken, PA: 1998.

[42] G.M. Ugiansky and J.H. Payer, "Stress Corrosion Cracking—The Slow Strain Rate Technique." AMERICAN SOCIETY FOR TESTING AND MATERIALS, paper no. 04-665000-27, (Toronto, Canada, 2-4 May, 1977)

[43]L. Willey, Aluminum 1, K. Horn, ed., ((Materials Park, OH: ASM, 1967) p. 174.

[44]M. Iskandar et. al., "The Effect of Varying Solution Heat Treatment Temperature, Natural Aging Treatment and Artificial Aging Treatment on the Mechanical Strength of 7249 Aluminum Alloy" (Report to the National Science Foundation, Research Experience for Undergraduates Program, Loyola Marymount University, Los Angeles, CA, August 2001).

[45]C.P. Ferrer, "Optimizing the Strength and SCC Resistance of Aluminum Alloys Used for Refurbishing Aircraft" (Trident Scholar project report, no. 281, United States Naval Academy, 2001).

[46]C.P. Ferrer, M.G. Koul, B.J. Connolly, A.L. Moran, "Utilization of Low Temperature Retrogression and Re-Aging (RRA) Heat Treatments to Improve Strength/SCC Properties for Thick Section Components of Aluminum Alloy 7075 for Aging Aircraft Refurbishment," CORROSION/2002, paper no. 02159, (Houston, TX: NACE, 2002).

[47] "Standard Practice for making and Using Precracked Double Beam Stress Corrosion Specimen." *Annual book of ASTM Standards,* Vol 03.02. West Conshohocken, PA: 2000.